Alkali-activated fly ash cured with pulsed microwave and thermal oven: A comparison of reaction products, microstructure and compressive strength

Shi Shi [a], Hui Li [b], Qizhi Zhou [a], Hongzhou Zhang [c], P.A.M. Basheer [d], Yun Bai [a],[*]

[a] Advanced & Innovative Materials (AIM) Group, Department of Civil, Environmental and Geomatic Engineering, University College London, Gower Street, London WC1E 6BT, United Kingdom
[b] College of Materials Science and Engineering, Xi'an University of Architecture and Technology, Xi'an 710055, PR China
[c] Centre for Research on Adaptive Nanostructures and Nanodevices (CRANN), Naughton Institute, Trinity College Dublin, Dublin 2, Ireland
[d] School of Civil Engineering, University of Leeds, Woodhouse Lane, Leeds LS2 9JT, United Kingdom

ABSTRACT

The reaction products and microstructure of an 8 M NaOH-activated fly ash (AAFA) cured with microwave and thermal oven curing were comparatively investigated. The results show that the formation of an Al-rich N-A-S-H gel with a flaky morphology and crystalline chabazite-Na between fly ash particles were favoured under the microwave curing, whilst a Si-rich N-A-S-H gel with a fibrilllar morphology and crystalline hydroxysodalite on the surface of fly ash particles were dominant under the thermal oven curing. The formation of these unique reaction products and microstructure under the microwave curing is attributed not only to the thermal effect of microwaves which can increase the temperature of AAFA volumetrically, but also to the non-thermal effects of microwaves which can promote the dissolution and diffusion of silica and alumina during the AAFA reaction process. This explains why AAFA can achieve a high early strength within a short period of microwave curing.

1. Introduction

Fly ash is a by-product from thermal fire power plant. Although some European countries, like Netherlands, Denmark and Italy have a fly ash utilization rate of 100 % or even a shortage of fly ash for construction application in PC concrete, fly ash utilization is only 25 % of the total production globally [1]. Especially, the top three producers, India, China and the USA have the utilization rate of 38 %, 45 % and 65 % respectively [1]. Therefore, techniques still need to be developed to increase the fly ash utilization rate in these countries. One of the promising techniques is alkali-activated fly ash (AAFA), through which the fly ash rich in alumina and silica can react with alkaline activators, such as sodium hydroxide and sodium silicate, to produce AAFA [2–4].

It is well accepted that the chemical reaction process of AAFA involves two main stages, namely, dissolution and polymerisation [5,6]. In the dissolution stage, the reactive components of SiO_2 and Al_2O_3 in fly ash are dissolved under a strong alkaline condition [7], whilst in the polymerisation stage, the dissolved reactive $Si(OH)_4$ and $Al(OH)_4^-$ polymerise to produce the main reaction product, sodium aluminosilicate hydrate (N-A-S-H gel), and a small number of zeolites [2], leading to the formation of a well-compacted cementitious matrix. These two

stages undergo simultaneously once fly ash particles are in contact with the alkaline solution [8], but each advances at different speed at different process time. It is generally believed that, in the early stage, the speed of the dissolution of SiO_2 and Al_2O_3 is much greater than that of the precipitation of N-A-S-H gel. As the reactions progress, the fly ash particles are then covered with the formed N-A-S-H gel, which can slow down the dissolution of SiO_2 and Al_2O_3, hindering the further formation of N-A-S-H gel. Since the aluminate species dissolve faster than silicate species [9], the initially formed N-A-S-H gel is an Al-rich gel. With the further dissolution of SiO_2 and Al_2O_3, the Al-rich gel starts to be converted into a Si-rich gel [10], resulting in an increase in the mechanical performance of AAFA. However, it is noteworthy that the chemical reaction and strength gain of AAFA at room temperature is slow. This is especially the case for *NaOH-activated AAFA*. As a result, thermal curing has been considered essential for the initiation of the chemical reaction and subsequent strength development of AAFA [11,12]. The prevailing curing method in the literature for AAFA is thermal curing in an electric oven at 85 °C. It normally takes >8 h for the early strength to reach above 20 MPa, depending upon the reactivity of the fly ash [13]. In thermal oven curing, the dominant heating mechanism is thermal radiation and conduction, where the heat transmits from the surface to the

core of the samples. It is slow and less efficient. Additionally, it could generate a thermal gradient throughout the sample [14], leading to thermal cracks and reduced strength development.

Compared to conventional thermal heating, such as the use of thermal oven, it is generally agreed that microwave heating is more efficient and requires less energy, which can heat the dielectric materials volumetrically [15]. Since all of the components of concrete, such as water, cement and aggregate, are dielectric materials, concrete itself has been considered as a dielectric material [16]. The dipolar molecules in the dielectric materials, particularly water, can vibrate by following the alternating electromagnetic field of microwave, which generates frictions between the molecules. In this way, microwave energy can be converted into heat energy quickly and volumetrically [15,17]. To explore the potential of using microwave heating as an alternative accelerated curing technique for cementitious materials, some pilot studies have been carried out in the past to cure Portland cement (PC)-based products [18–25]. Among these, Watson [18] is probably the first researcher reported in the literature who applied microwave heating to cure PC concrete (100 × 100 × 100 mm) in 1968. In this work, a compressive strength of 7.7 MPa was obtained after only 2 h of curing in a commercial, domestic microwave oven, whilst the compressive strength obtained after 24 h of curing in moist air was 8.0 MPa. Followed by Watson's pioneering work, Wu et al. [19] used a domestic microwave oven (full power of 650 W) to cure PC mortar samples (40 × 40 × 160 mm) immediately after casting. However, only the power level of 150 W was employed, because at higher power levels the cement slurry splashed out which was possibly due to the violent evaporation of water. To effectively avoid this, Hutchison et al. [20] introduced a water load (i.e. extra water put aside the specimen in the microwave oven) into a domestic microwave oven when PC mortar samples (40 × 40 × 160 mm) were cured immediately after casting. As some of the microwaves were absorbed by the water load, the splash of cement slurry was avoided. Additionally, a delay period (i.e. initial curing at room temperature prior to thermal curing) before microwave curing was found to be useful for addressing the splashing issue and further increasing the strength of PC samples [21–23]. Based on the previous research on PC-based systems, it can be clearly seen that microwave curing can significantly reduce the curing duration, demonstrating a great potential to be an alternative accelerated curing technique for cementitious materials.

Although microwave curing has been confirmed to be efficient for curing PC-based products, research on curing AAFA with microwave heating is limited [26–28]. Chindaprasirt et al. [27] applied a hybrid curing method (i.e. microwave + thermal oven) to cure waterglass-activated AAFA mortar samples (50 × 50 × 50 mm) and the highest strength was obtained after microwave curing at 90 W for 5 min and a subsequent thermal oven at 65 °C for 12 h. In a following study, Graytee et al. [26] applied a domestic microwave oven to cure waterglass-activated AAFA paste samples (50 × 50 × 50 mm). They compared the effects of different microwave power levels, namely, 200 W, 300 W, 400 W and 600 W, and found that 200 W was the most suitable power level, which was then used to compare with oven curing at 90 °C and 120 °C. The results showed that all the microwave cured AAFA samples developed higher strength than the thermal oven cured samples after the same curing duration. However, waterglass has a high carbon footprint and its usage in AAFA system also causes the issues of shrinkage and cracking [29–31]. Thus, NaOH is often a preferred alkaline activator for AAFA. In 2010, Somaratna et al. [28] reported the first investigation on curing *NaOH-activated AAFA* with a domestic microwave oven. In their study, the AAFA mortar samples (50 × 50 × 50 mm) were cured at varying percentages of full microwave power level for different curing durations after a 12-hour delay period. They reported that 30 %, 60 % and 100 % of full microwave power (1200 W) caused severe cracks inside the sample, which is possibly due to the evaporation of water and overheating. Nonetheless, the compressive strength gained with a 2-hour microwave curing at 240 W (20 % of full microwave power) was higher than that with 48-hour thermal oven curing at 75 °C, indicating

microwave curing has a good potential for manufacturing *NaOH-activated AAFA* products. It is worth highlighting that in the above studies, the higher and faster strength development from microwave cured AAFA samples was attributed by the authors simply to the volumetric heating of microwaves (i.e. **thermal effect**). Whilst this is certainly true due to the enhanced reaction at higher temperature (similar to those reported for other accelerated curing techniques), ultimately the strength is determined by the reaction products and microstructure of the matrix formed [10,32]. On the other hand, it is well-known that, in addition to the thermal effect, the electromagnetic field of microwaves also generates **non-thermal effects**, which could, for example, lead to improved dissolution of the matter in liquid [33]. It has been reported that during the process of synthesising zeolites under microwave radiation, the dissolution of SiO_2 and Al_2O_3 can be accelerated [34]. In addition, it was found that the diffusion of dissolved silica and alumina can be improved under microwave radiation during the synthesis of zeolites [4,33,35]. As zeolite synthesis shares some similarities with the alkaline activation of fly ash, similar effects might exist in curing AAFA with microwave heating. Therefore, it is possible that not only the dissolution of SO_2 and Al_2O_3 from fly ash particles can be enhanced under microwave radiation, the diffusion, nucleation, growth/precipitation and crystallisation processes could also be affected. This may lead to the formation of different reaction products and microstructure of AAFA which could potentially explain the increased strength obtained within a short curing duration as reported in the literature. However, to date, the reaction products and microstructure of AAFA cured with microwave curing have not been thoroughly studied, hence their influence on mechanical properties cannot be clearly elucidated at present.

Therefore, this study investigated the reaction products and microstructure of a microwave-cured *NaOH-activated AAFA* and their influence on the early strength development of AAFA. Similar to the previous studies reported in the literature, only part of the full power was employed in the current study together with a water load, in order to avoid both the splashing issue and cracks caused by overheating under microwave curing. However, instead of using the pre-fixed power levels provided by commercial, domestic microwave ovens, a pulsed microwave heating regime consisting of 'power-on' and 'power-off' duty cycles based on the full power of microwave oven was adopted in this study. This is because compared to the pre-fixed power levels, the pulsed microwave regime is more flexible and more energy efficient as has already been proved in the food industry [36,37]. The reaction products of the AAFA were characterised by X-ray powder diffraction (XRD), Fourier-transform infrared spectroscopy (FTIR) and thermal gravimetric analysis (TGA), whilst the microstructure was studied by scanning electron microscopy (SEM), transmission electron microscopy (TEM) and mercury intrusion porosimetry (MIP) analyses. These data for *NaOH-activated AAFA* were also compared between the pulsed microwave curing and the conventional thermal oven curing. The results are then used in this paper to establish how and why a high compressive strength of *NaOH-activated AAFA* could be achieved within a short period of time by microwave curing.

2. Experimental

2.1. Materials

A Class F fly ash from Weihe coal power plant, Shaanxi, China was used in this work. Table 1 gives its chemical composition and Fig. 1 shows its particle size distribution. Due to the high content of silica and alumina in the amorphous phase, the Class F fly ash is ideal for alkaline activation [38]. The mean particle size of the fly ash used in this project was 18 μm and the percentage of particles <45 μm was 88.55 %. Sodium hydroxide used was supplied by ReAgent, the UK, with a purity of 95 % at industrial grade.

Table 1

Chemical composition of the Class F fly ash used in this study (wt/%).

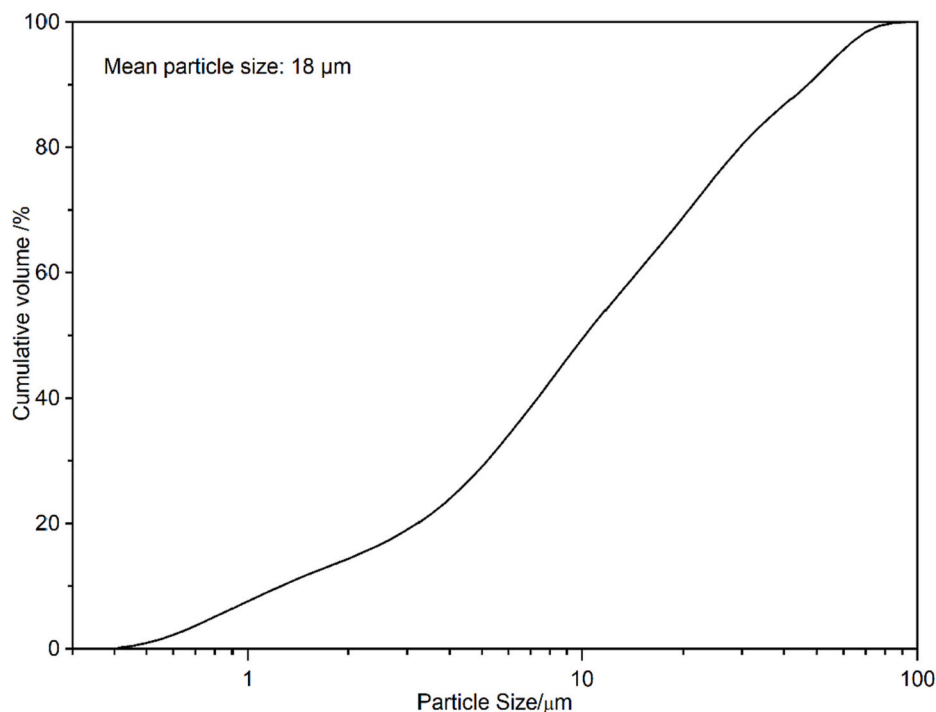| SiO_2	Al_2O_3	Fe_2O_3	CaO	Na_2O	MgO	K_2O	SO_3	P_2O_5	TiO_2	Other	LOI
49.29	30.55	5.55	5.96	0.74	0.81	1.38	0.63	0.21	1.08	0.33	1.87

Fig. 1. Particle size distribution of fly ash.

2.2. Preparation of test samples

The AAFA paste was prepared by mixing the fly ash and 8 M NaOH solution at a solution to fly ash ratio of 0.3. Two types of three-gang moulds were used for microwave curing and thermal oven curing, i.e., microwave transparent PEEK moulds (Fig. 2) and steel moulds. The dimension of the samples was 25 × 25 × 25 mm.

Prior to both the thermal oven curing and the pulsed microwave curing, a 24-h room temperature (20 ± 1 °C) curing (i.e. delay period) was applied, which can not only reduce slurry splashing in microwave curing, but also enhance the dissolution of SiO_2 and Al_2O_3 from fly ash [7,28]. After the 24-h curing at room temperature, the samples were cured in a thermal oven and a domestic microwave oven, respectively, by following the curing regimes described below:

- Thermal oven curing: the thermal oven curing at 85 °C was adopted as the control in this study because this curing regime is widely used in the literature. The AAFA samples were cured for 2 h, 4 h, 7 h and

24 h in the pre-heated oven before the corresponding tests were carried out (as detailed in the section below).

- Pulsed microwave curing: a Panasonic domestic microwave oven with a full power of 600 W was used for microwave curing. The pulsed microwave curing regime, which was established from preliminary trials, was used in this study and this was achieved through the control of 'power-on' and 'power-off' duty cycles based on the full power of the microwave oven during the microwave curing process. The pulsing ratio (PR) is defined as $PR = (t_{on} + t_{off})/t_{on}$ [36], where t_{on} and t_{off} are the 'power-on' and 'power-off' durations of the microwave pulses per duty cycle, respectively.

The PR employed in this study was 20 and each cycle lasted for 2 min, namely, $t_{on} = 6$ s and $t_{off} = 114$ s in each cycle, which is equivalent to 5 % of the full microwave power level. The AAFA samples were cured for 10 cycles, 20 cycles, 30 cycles and 40 cycles in the microwave oven. In addition, a water load of 300 g was applied which was proved to be able to totally eliminate the slurry splash from the trials.

To avoid moisture loss and provide a moist environment during the thermal oven curing and pulsed microwave curing, the fresh AAFA samples were wrapped together with the moulds with three layers of cling film and three layers of water saturated wet hessian, which were then sealed in plastic bags during the thermal oven curing and pulsed microwave curing. Following both the thermal oven curing and the pulsed microwave curing, all the samples were cooled down to room temperature (20 ± 1 °C) before carrying out the compressive strength test. The debris collected after the compressive strength test for carrying out both the analytical and microstructural characterisation was treated with acetone to arrest further chemical reactions. After drying in desiccator under vacuum, part of the debris was ground into fine powder


Fig. 2. PEEK mould.

passing 63 μm sieve for XRD, FTIR, and TGA. The other selected debris were used for SEM, TEM and MIP analyses.

2.3. Analytical methods

Before carrying out various physical and microstructural analyse, the compressive strength of the AAFA paste samples was determined after thermal oven curing for 2 h, 4 h, 7 h and 24 h and after microwave curing for 10 cycles, 20 cycles, 30 cycles and 40 cycles. At each age, three $25 \times 25 \times 25$ mm cubes were crushed and the average compressive strength of the three cubes was reported as the compressive strength.

Reaction products were characterised by using a number of analytical equipment. The XRD patterns of the AAFA powder samples were obtained with a RICOH D-MAX/2500PC Diffractometer using
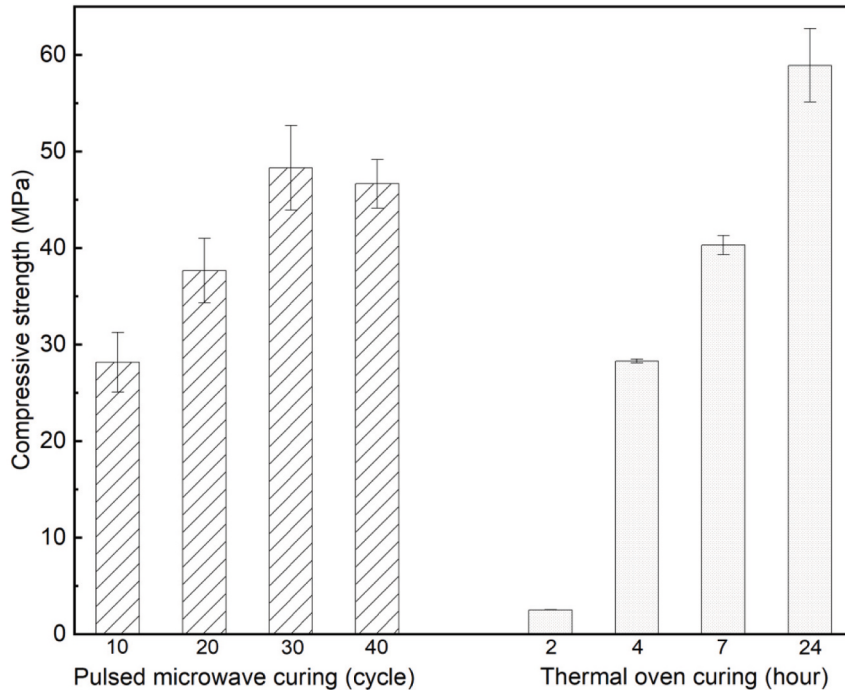
a. Compressive strength under different curing methods
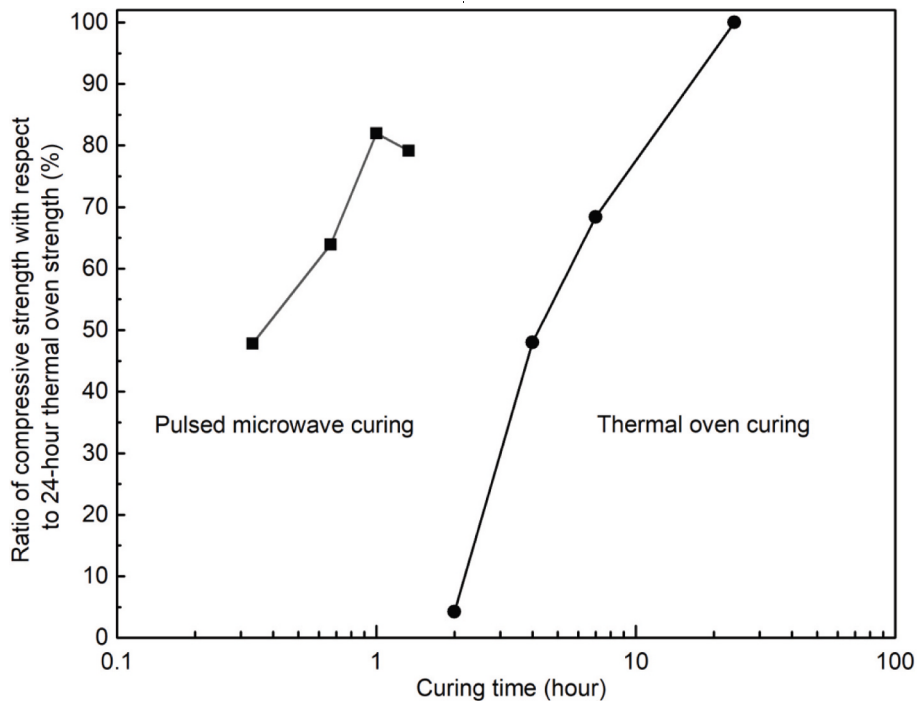
b. Development of compressive strength over curing duration

Fig. 3. Compressive strength of AAFA.

monochromatic CuK$_\alpha$ radiation. The scan was carried out in the range of 5-70° (2θ) at a speed of 2°/min. The FTIR spectra of the AAFA powder samples were obtained on a Perkin Elmer Spectrum One Spectrometer over the range of 1250-450 cm^{-1}. Specimens were prepared by mixing 1 mg of the AAFA powder sample with 300 mg of KBr and then pressed into a pellet. The TGA of the AAFA powder samples was carried out using a TGA/DSC-1600 instrument. The temperature programme used was 10 °C/min between 50 °C and 1000 °C, during which the furnace was purged with N$_2$ at 100 ml/min. The amount of amorphous phase in the original ash was determined by acid attack with 1 % HF [39,40], whilst the amount of amorphous phase after the activation process in AAFA was determined by acid attack with 1:20 HCl [41,42].

A FEI Quanta200 SEM was applied to examine the morphology and microstructure of the hardened AAFA paste samples. The debris obtained after the compressive strength test was coated with gold for the SEM analysis. A FEI-Titan-80 TEM with EDX analysis was used to examine the morphology and chemical compositions of the reaction products. The fine AAFA debris were dispersed in ethanol and holey carbon coated copper grids were used for TEM/EDX analysis. An AUTOPore IV 9500 Micromeritics Instrument was used for MIP analysis to obtain the pore size distribution of the hardened AAFA samples. The AAFA debris was placed in a vacuum oven at 40 °C overnight prior to the test.

An infrared camera, FLIR E60bx, was used to measure the temperature of the AAFA sample immediately upon completion of both the thermal oven curing and the microwave curing. The 25 × 25 × 25 mm cubes were split into two halves from the middle of the height and the temperature inside the AAFA sample was measured. A TAM Air 8-channel calorimeter from TA Instruments was used to monitor the heat evolution of AAFA. The fly ash and NaOH solution were preheated at 85 °C overnight before they were mixed and loaded into the calorimeter. The test was carried out for 24 h at 85 °C.

3. Results

3.1. Compressive strength

Fig. 3a shows the compressive strength development of AAFAs produced with both the thermal oven curing and the pulsed microwave curing. It can be clearly seen that, prolonged curing time (up to 24 h) has a positive effect on the development of compressive strength of AAFA under thermal oven curing at 85 °C. Although the early-age compressive strength of AAFA was only 2.5 MPa after 2 h of thermal oven curing (which is only 4.2 % of the compressive strength developed after 24 h of thermal oven curing), the compressive strength reached 28.3 MPa after a 4-hour thermal oven curing, and then further increased to 40.3 MPa after a 7-hour thermal oven curing. The highest compressive strength of 58.9 MPa was obtained after 24 h of thermal oven curing, which is around 100 % increase in compressive strength compared to the strength developed after a 4-hour thermal oven curing. For microwave curing, the compressive strength of AAFA samples also increased with increased curing duration. After 10 cycles of pulsed microwave curing (i. e., lasted for 20 min), the compressive strength of 28.2 MPa was obtained, which is equivalent to the compressive strength developed after a 4-hour thermal oven curing and 47.8 % of that after a 24-hour thermal oven curing. After 20 cycles of pulsed microwave curing (i.e., 40 min), the compressive strength achieved 37.6 MPa, which is around 63.9 % of the compressive strength developed after the 24-hour thermal oven curing. The development of compressive strength reached a peak of 48.3 MPa after 30 cycles of pulsed microwave curing (i.e., 1 h), which is 82 % of the compressive strength developed after the 24-hour thermal oven curing. A slightly lower compressive strength of 46.6 MPa was noticed after 40 cycles of pulsed microwave curing (i.e., 1 h 20 min), even though statistically not much different from the AAFA cured with 30 cycles (as can be recognised from the error bars), indicating that the compressive strength development reached a plateau – a feature of

AAFA materials under accelerated curing [7]. Taken the strength developed after 24 h of thermal oven curing as benchmark, Fig. 3b shows the strength development ratio over different curing durations under the two curing methods. It can be clearly seen that compared to the thermal oven curing, the pulsed microwave curing can significantly accelerate the strength development, leading to a dramatic reduction in the curing duration for AAFA. For example, it took only 10 cycles (i.e., 20 min) for the pulsed microwave curing to reach 28.2 MPa. However, it took 4 h for the thermal oven curing to reach a similar compressive strength (28.3 MPa). This represents a 91.7 % reduction in curing duration. Similar trends can be noticed from 20, 30 and 40 cycles of the pulsed microwave curing. In particular, after only a 1-hour pulsed microwave curing (i.e., 30 cycles), the compressive strength of AAFA reached 48.3 MPa, whilst at the same curing duration, there was almost no strength being developed under the thermal oven curing (only 2.5 MPa being achieved after a 2-hour thermal oven curing). Furthermore, as the pulsed microwave curing consisted of a 'power-on' and a 'power-off' durations, with a pulsing ratio of 20 being employed in this study, the actual microwave heating time for AAFA was even shorter (i.e., 1 min for every 10 cycles).

From the above comparison of the compressive strength development cured with the pulsed microwave and the thermal oven, it is evident that microwave curing has a great advantage in reducing the curing duration and energy consumption in the manufacture of AAFA products. However, as discussed before, how and why this fast strength development has been achieved by microwave curing is still not well understood in the literature. Hence, the reaction products and microstructure of the AAFAs obtained the highest compressive strength under these two different curing methods, namely the samples cured with the thermal oven curing for 24 h (OV24) and the pulsed microwave curing for 30 cycles (MW30), were further characterised and compared (as reported below), with an attempt to achieve a better understanding of the mechanisms involved in microwave curing. However, it should be noted that curing duration for OV24 was 24 h, whilst it was only 1 h for MW30 (equivalent to only 3 min of effective microwave heating time).

3.2. Reaction products

3.2.1. XRD

Fig. 4 presents the XRD patterns of the raw fly ash and the two AAFA samples under different curing methods. The raw fly ash is dominated by
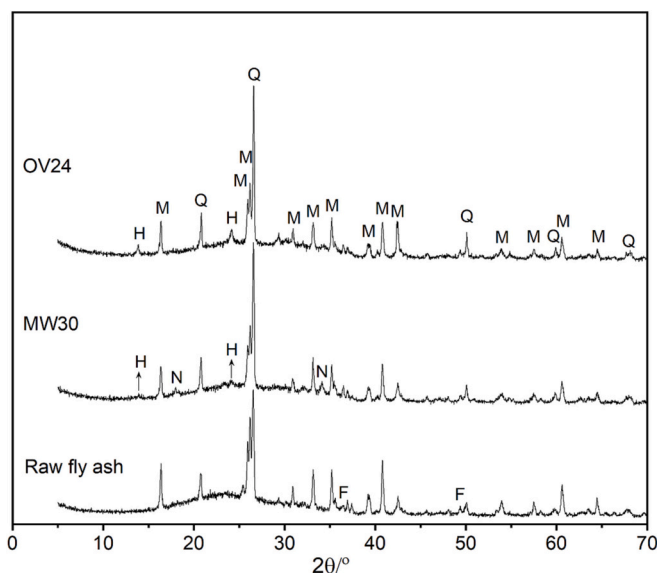

Fig. 4. XRD patterns of raw fly ash and AAFA (Q-quartz, M-mullite, F-hematite, H-hydroxysodalite, N-chabazite-Na).

amorphous phases (as indicated by a hump at 17-33° 2θ) with a series of minor crystalline phases, such as quartz, mullite and hematite. After alkaline activation, the crystalline phases detected in the raw fly ash remained unchanged in both AAFA samples, while the area under the hump decreased, indicating that the amorphous phase in the raw fly ash was consumed during the alkaline activation process. In addition, two new peaks appeared at 13.8° and 24° 2θ in MW30 which are assigned to hydroxysodalite (atomic Si/Al ratio = 1), whilst the other two new peaks at 18.0° and 34.2° 2θ in MW30 can be attributed to chabazite-Na (atomic Si/Al ratio = 2). Compared to the pulsed microwave curing, only hydroxysodalite (atomic Si/Al ratio = 1) was identified in the AAFA cured with thermal oven, whilst chabazite-Na was not found. This finding is in agreement with previous findings reported for the AAFA cured with thermal oven in the literature [7]. Additionally, it should be noted that although hydroxysodalite was identified in both AAFA samples, its intensity in MW30 is much weaker.

3.2.2. FTIR

Fig. 5 presents the FTIR spectra of the raw fly ash and two AAFA samples (OV24 and MW30). The bands at around 3400 cm^{-1} were associated to the O—H (hydroxyl group) stretching vibration and the bands at around 1600 cm^{-1} were associated to the H—O—H (water molecule) bending vibration. A wide band observed at 1087 cm^{-1} in the raw fly ash was associated with T-O (T = Al, Si) asymmetric stretching vibrations. The presence of quartz and mullite was associated with the bands at 795 cm^{-1} and 554 cm^{-1} in the raw fly ash, respectively, and both of these bands barely changed after activation, which is consistent with the XRD results. This suggests that the inert crystalline phases, quartz and mullite, did not take part in the reaction of alkaline activation [43]. In contrast, the T-O band at 1087 cm^{-1} became sharper and shifted to lower frequencies at 1007 cm^{-1} in MW30 and at 1010 cm^{-1} in OV24. This band shift has been considered as the formation of N-A-S-H gel in AAFA. It is interesting to notice that the T-O band shifted towards a lower frequency in MW30 than that in OV24, implying more Al-rich N-A-S-H gels were formed under the microwave curing [32]. Two new bands appeared around 665–670 cm^{-1}, which was interpreted to be the presence of hydroxysodalite in MW30 and in OV24 respectively, and another new band associated with zeolite specie appeared at 735–740 cm^{-1} in MW30 is assigned to chabazite-Na [13,32], which is in good agreement with the XRD results reported in the current study.

3.2.3. TGA

The TG/DTG curves of the AAFAs manufactured using the two different curing methods are shown in Fig. 6. From the TG curves in Fig. 6a, a higher total weight loss from OV24 (7.5 %) than that from MW30 (6.4 %) over the entire temperature range can be clearly identified. As evident from the DTG curves in Fig. 6b, some obvious differences can be identified from the major peaks of the two samples between 100 °C and 200 °C which can be attributed to the dehydration of the main reaction product, N-A-S-H gel, formed in AAFA. In MW30 the dehydration of N-A-S-H gel led to the formation of a broad peak, while a sharp peak centred around 150 °C was formed in OV24 [44]. The areas of these two DTG peaks corresponding to the weight loss of N-A-S-H gel in MW30 and OV24 are around 2.9 % and 3.9 %, respectively. It is worth highlighting that the above results correlate well with the amount of the amorphous phase measured in both MW30 (37.36 %) and OV24 (38.66 %) samples using acid attack with 1:20 HCl. Whilst the above two methods give different values, the general trends are consistent, i.e., most of the N-A-S-H gel formed in OV24 over 24 h can be formed under microwave curing within only 1 h. On the other hand, the weight loss associated with the zeolite phases formed under different curing methods can also be noticed from the DTG analysis. Specifically, the weight loss between 340 and 520 °C in MW30 could be attributed to the release of chemically bound water from chabazite-Na [45], whilst the weight loss between 520 and 690 °C in both OV24 and MW30 could be attributed to the decomposition of metal-OH groups from hydroxysodalite [46]. It must be stressed that above results can further strengthen the findings from XRD and FTIR (as presented above) in which both chabazite-Na and hydroxysodalite have been clearly identified. Nonetheless, the most important conclusion which can be drawn from the TG study is that equivalent amount of N-A-S-H gel formed under thermal oven curing for 24 h can be formed under microwave curing within only one hour. This implies that one of the possible reasons causing the fast strength development of the microwave cured AAFA is due to the quick and increased formation of N-A-S-H gel within a short period of time under the actions of alternating electromagnetic fields of microwaves as detailed below in Discussion.

3.3. Microstructure

3.3.1. SEM

Fig. 7 shows the morphology of the fractured surface of two AAFA samples cured with microwave (a-1 to d-1) and thermal oven curing (a-2 to d-2) techniques. As can be clearly seen from Fig. 7a-1 and Fig. 7a-2, in general, both samples featured heterogeneous morphology, but compacted texture. In particular, it can be observed that the reaction products not only covered or partially covered the surface of fly ash particles, but also filled in the regions between the fly ash particles, leading to the formation of a compacted cementitious matrix. The co-existence of reacted fly ash particles with unreacted particles can also be observed in both matrices. However, comparing Fig. 7b-1 and Fig. 7b-2, it can be noticed that the reaction products formed in MW30 showed granular and circular morphology with the products mainly precipitated in the regions between fly ash particles, whereas those in OV24 are mainly dominated by flake structure and the reaction products were mainly formed in the close vicinity of fly ash particles. It must be highlighted that the morphology and microstructure of OV24 in Fig. 7b-2 is very similar to those reported from the thermal oven cured AAFA in the literature [5]. Additionally, as shown in Fig. 7c-2, the products precipitated on the surface of the sample OV24 is much thicker and denser than that on MW30 (Fig. 7c-1). It is also interesting to notice that some long fibrous reaction products were found in MW30 (Fig. 7d-1), which could be attributed to sodium carbonate phases observed in previous research [47]. In contrast, some short needles with a star shape were formed in OV24 (Fig. 7c-2). Furthermore, there were more small crystalline
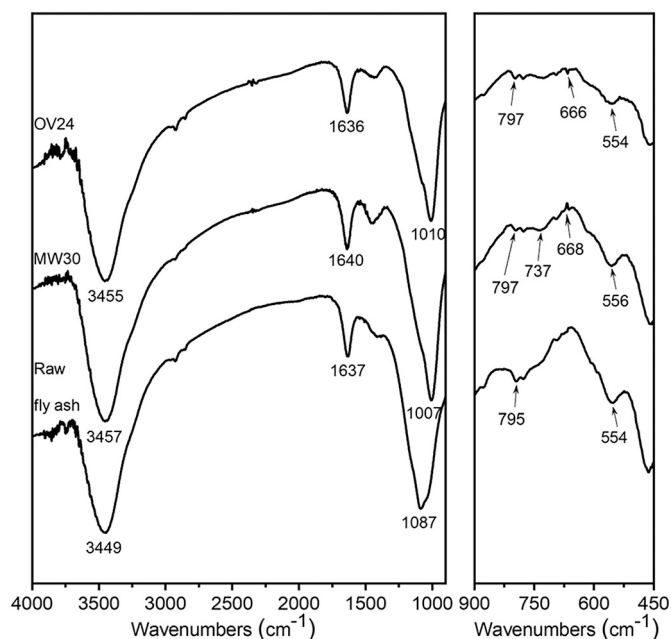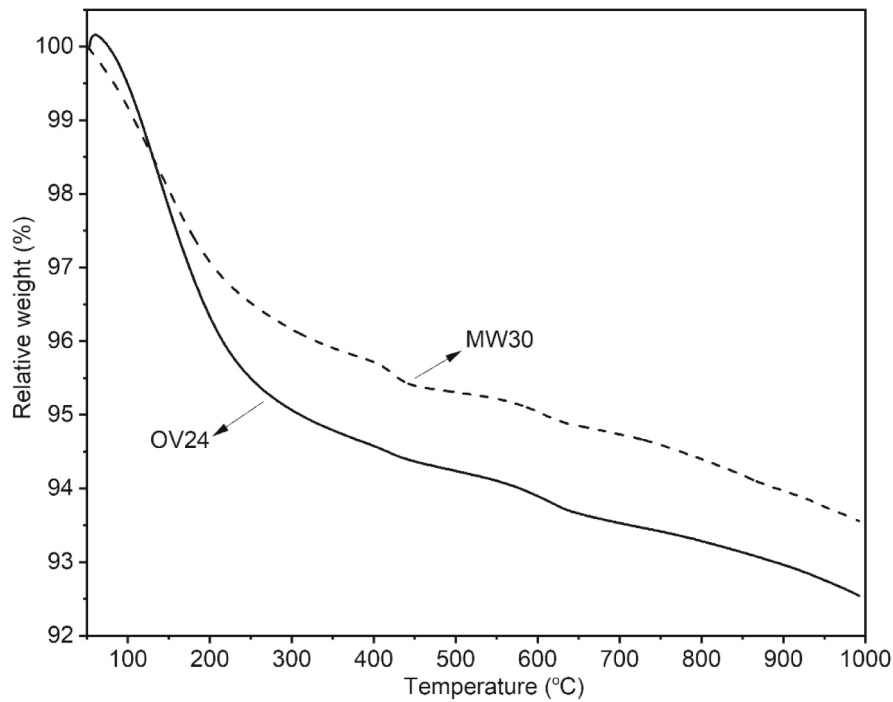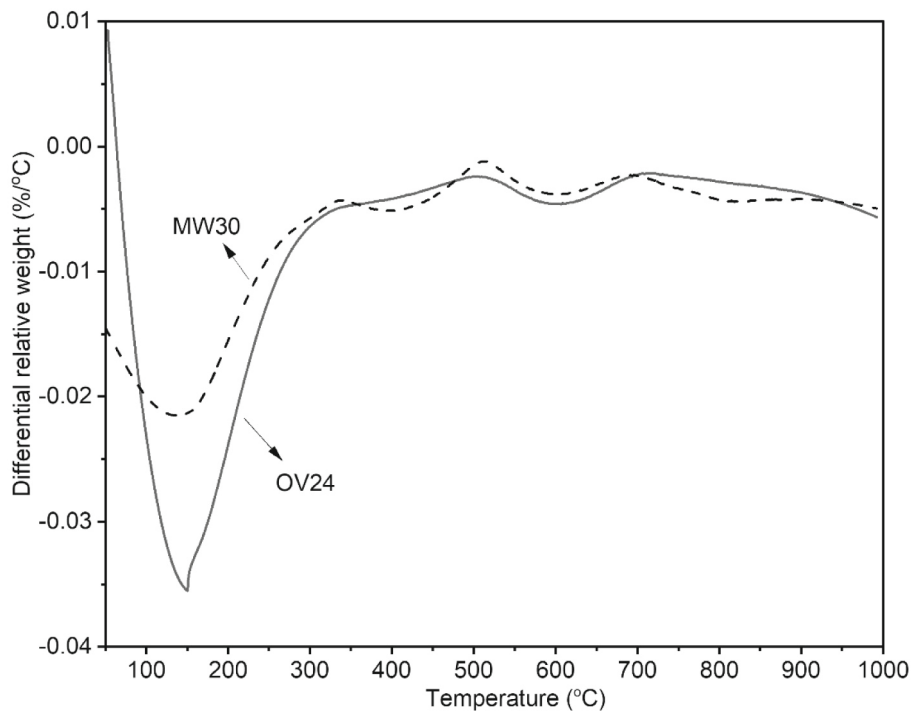

Fig. 5. FTIR spectra of raw fly ash and AAFA (4000–900 cm^{-1} and 900–450 cm^{-1}).

a. TG curves

b. DTG curves

Fig. 6. TG/DTG analysis of AAFA.

particles observed on the surface of fly ash in MW30 than that in OV24, which implies that the crystallisation process was promoted by microwave curing compared to conventional thermal curing.

3.3.2. TEM

Fig. 8 shows the TEM images of the fly ash particles in AAFA under the microwave curing and the thermal oven curing. Different features in the morphologies of fly ash particles can be clearly seen. Highly irregular morphology of the broken fly ash was found under the microwave curing (Fig. 8a), which is a typical feature observed from the microwave cured AAFA. In addition, both the surface and interior of the broken fly ash particle were covered by some reaction products. The presence of
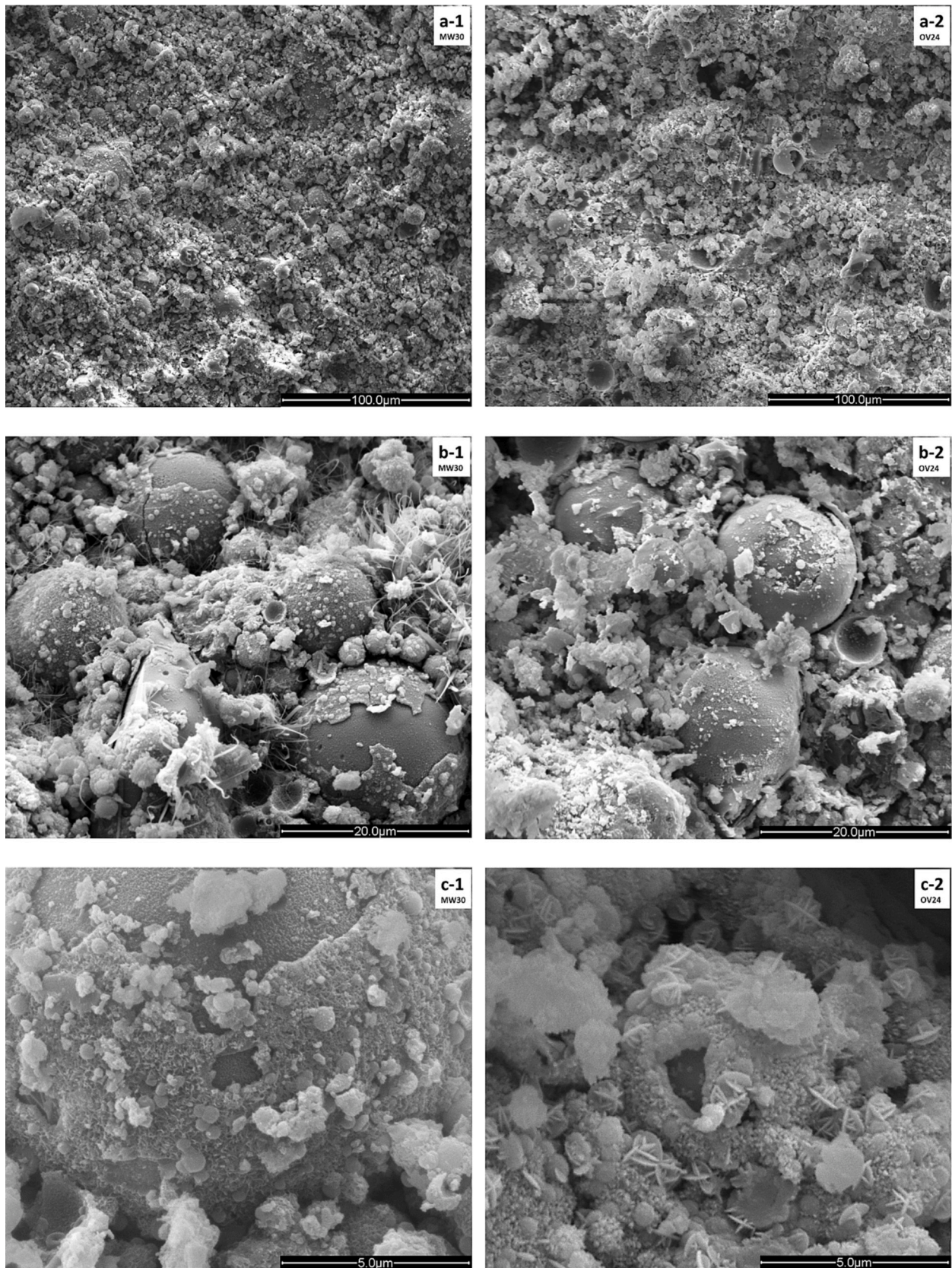
Fig. 7. SEM images of AAFA samples: (a-1) and (b-1) showing heterogeneous morphology of AAFA. (a-2) and (b-2) showing reaction products formed between fly particles. (a-3) and (d-3) highlighting the reaction products formed on the surface of fly ash particles. (a-4) and (d-4) presenting some crystalline particles in AAFA.
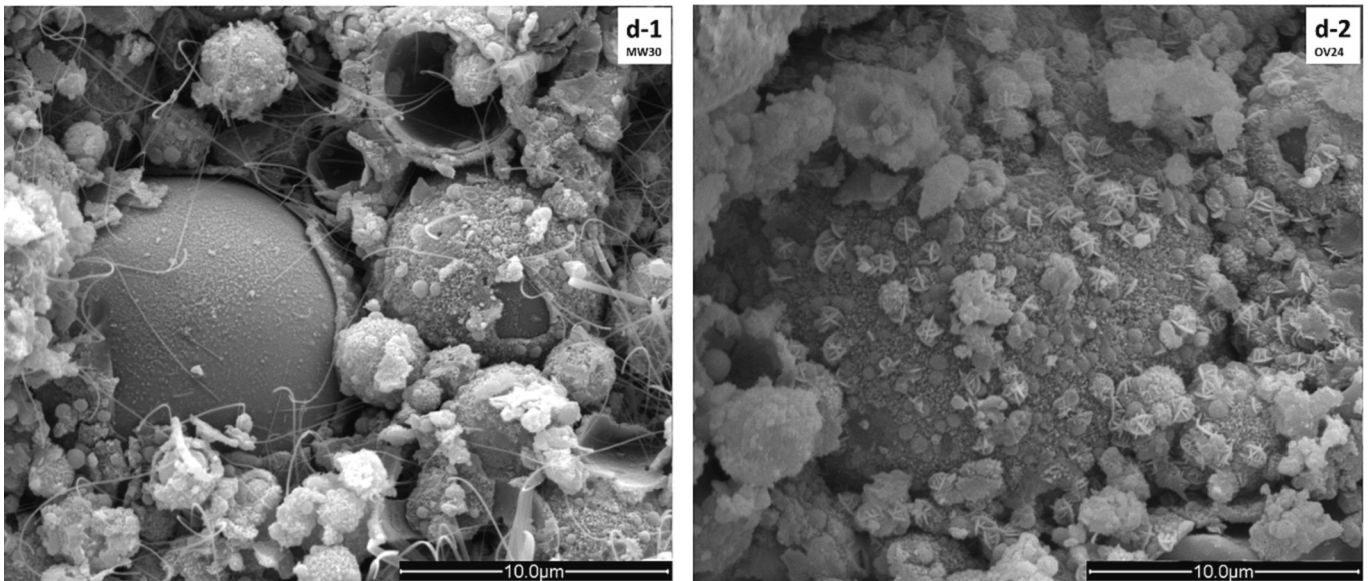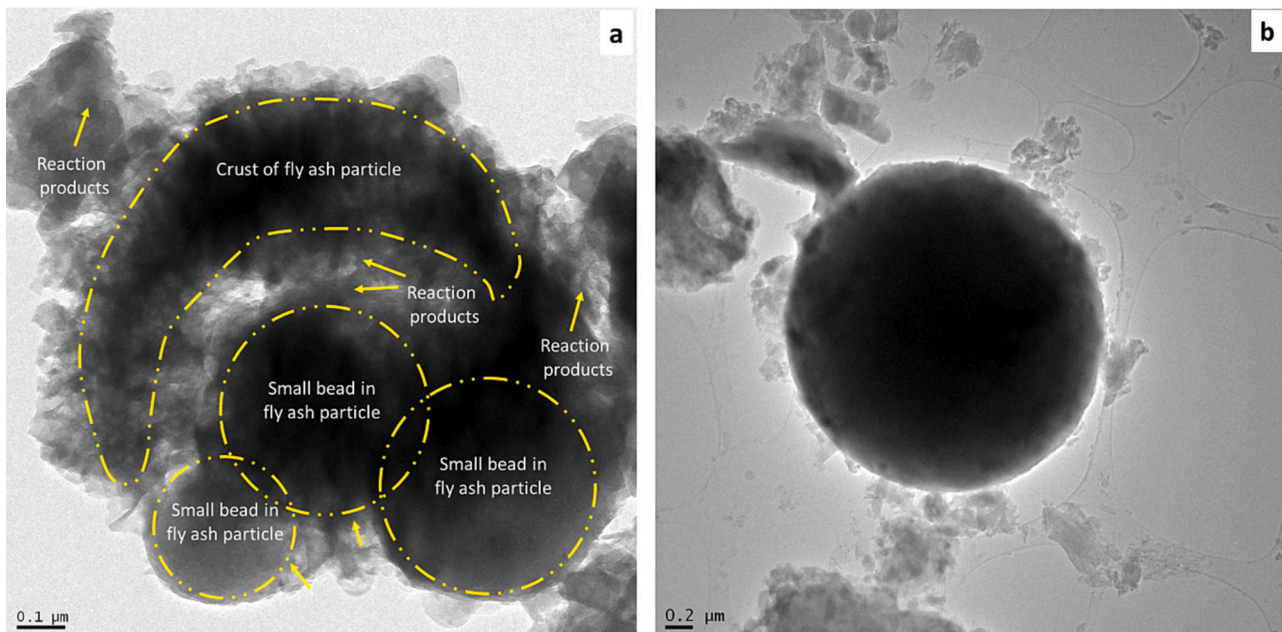
Fig. 7. (*continued*).

Fig. 8. TEM images of activated fly ash particles: (a) showing a broken fly ash particle encompassing small beads and reaction products formed inside and outside of the particles in MW30 and (b) presenting a spherical fly ash particle with reaction products formed on the surface of the fly ash particle in OV30.

considerable broken fly ash particles could be primarily attributed to the volumetric heating of microwaves, under which the fly ash particles could be heated from inside, leading to the possible internal expansion. Additionally, the magnetic beads existing in fly ash particles [48] which have a high capacity in absorbing microwaves, can also result in a fast local temperature rise and the breakdown of the fly ash particles due to the enhanced local stresses [49]. Consequently, the dissolution of the reactive silica and alumina can be promoted, benefiting the subsequent polymerisation (as further discussed below). In contrast, under the thermal oven, the majority of the fly ash particles still maintained the spherical morphology with the reaction products only formed on the surface (Fig. 8b).

To understand the effect of different curing methods on the reaction of fly ash particles, the partially reacted fly ash particles and the main reaction product, N-A-S-H gel, were further characterised by TEM/EDX

and the micrographs are shown in Fig. 9. As can be noticed, the spherical morphology of the fly ash particle in MW30 (Fig. 9a-1) is featured with a reaction rim of 200-250 nm thickness, surrounding the dark unreacted fly ash particle. Additionally, the reaction rim showed a diffused halo which might be caused by the increased diffusion of the reaction products formed around the fly ash particles. Whilst similar morphology can be observed from the fly ash particle cured with thermal oven (Fig. 9a-2), the thickness of the reaction rim, which has a clear-cut edge, is only about 100-150 nm. Although similar morphology of fly ash particle has also been reported in the literature [50], the diffused halo and the thicker reaction rim observed in the current study under the microwave curing would indicate that different reaction mechanisms must have been involved under these two curing methods. Furthermore, it can be seen that although the N-A-S-H gel formed in both MW30 and OV24 showed a crumpled foil-like morphology, the MW30 showed a coarser
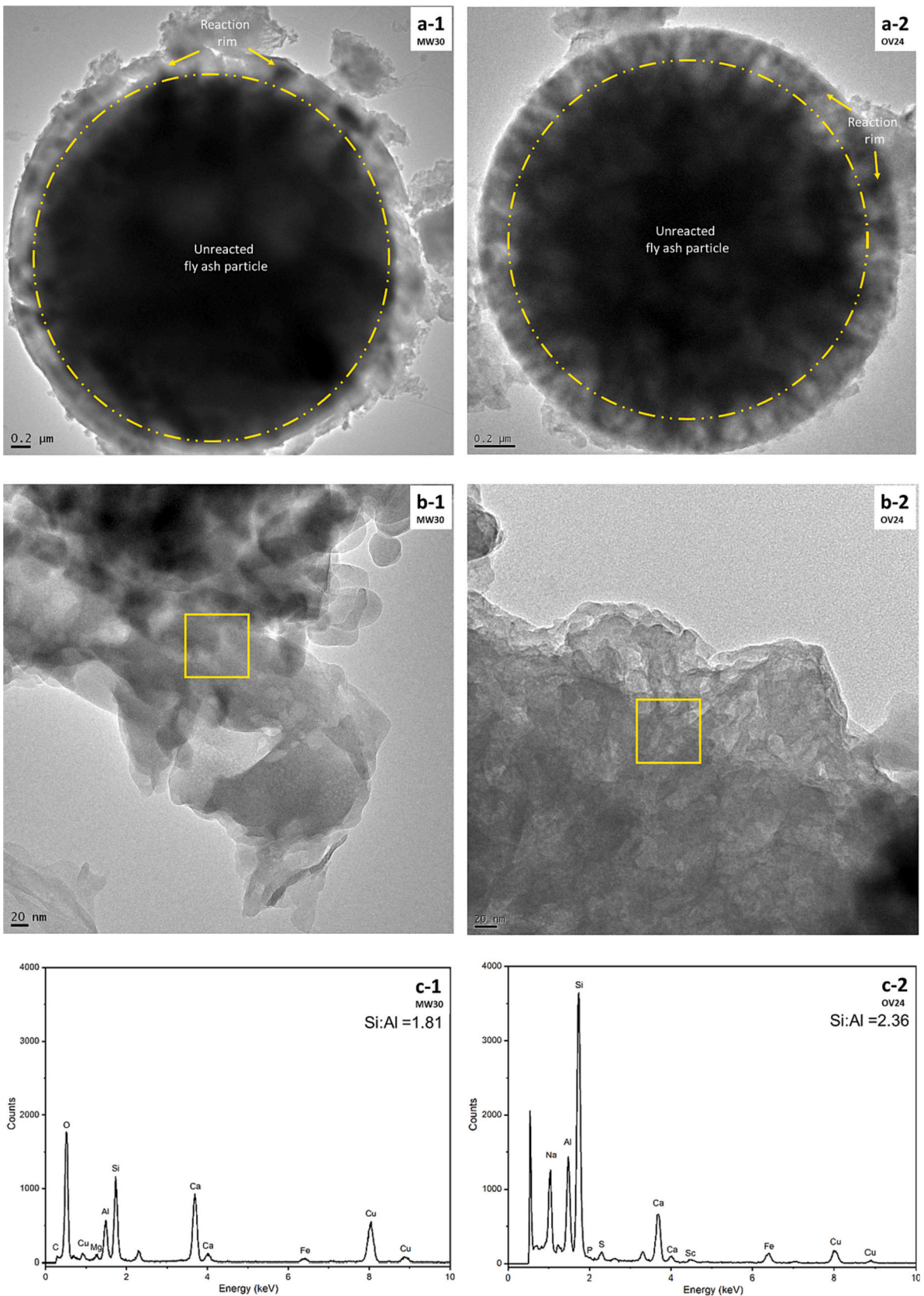
Fig. 9. TEM images of N-A-S-H gel formed in AAFA: (a-1) and (a-2) showing fly ash particles with reaction rims. (b-1) and (b-2) showing the N-A-S-H gel formed in AAFA. (c-1) and (c-2) giving the atomic Si/Al ratio of N-A-S-H gel in AAFA. (d-1) and (d-2) highlighting the difference in the structure of N-A-S-H gel.
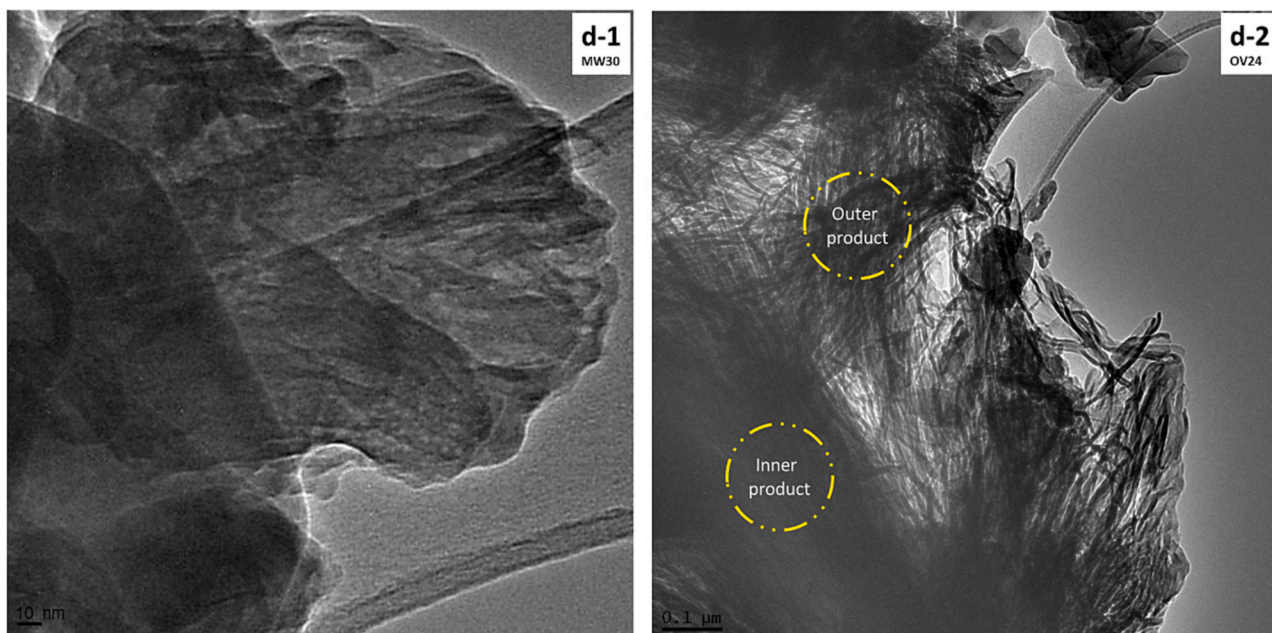
Fig. 9. (*continued*).

and porous N-A-S-H gel (Fig. 9b-1), compared to the finer and compacted N-A-S-H gel formed in OV24 (Fig. 9b-2). This observation corroborates well the findings from the SEM characterisation in which the reaction products formed in MW30 was found to be more porous than that in OV24. Additionally, this finding is also in good agreement with the MIP results (to be discussed in detail below) in which more fine pores was identified in OV24. Although the higher degree of maturity of OV24 might have contributed to this more refined pore structure, the unique thermal and non-thermal effects of microwave curing could have also caused the porous structure of MW30 (to be further discussed in the Discussion section). On the other hand, the EDX analysis indicate that the finer N-A-S-H gel in OV24 showed a higher atomic Si/Al ratio of 2.36 (Fig. 9c-1), compared to that of 1.81 in MW30 (Fig. 9c-2). This result is consistent with the findings from FTIR which again indicates that the microwave curing can facilitate the formation of an Al-rich N-A-S-H while the thermal oven curing may benefit the formation of a Si-rich gel. Fig. 9d-1 and Fig. 9d-2 further compare the morphologies of the two N-A-S-H gels formed under microwave curing and thermal oven curing. The flaky N-A-S-H gel from microwave cured AAFA sample showed an interwoven structure with a relatively, uniformly distributed texture, whist the fibrillar N-A-S-H gel from thermal oven cured AAFA demonstrated a denser inner product and a loose outer product. It should be noted that it is now widely accepted that, during the gel formation in AAFA, there is a transition of N-A-S-H gel from Al-rich phase (Gel 1) to Si-rich phase (Gel 2) [10]. As a result, the initially formed N-A-S-H gels has a lower Si/Al (i.e., higher Al/Si) ratio. However, it should be noticed that the Gel 1 in thermal oven cured AAFA usually has a Si/Al ratio of approximately one. In the current study, the Si/Al ratio of the N-A-S-H gel in MW30 is 1.81. This indicates that whilst the short duration of microwave curing could partly explain this Al-rich nature, something else might have also played a role in the gel formation under microwave curing. This will be discussed in detail in the Discussion section below.

Fig. 10 shows the TEM images of the mullites inside fly ash particles. It can be seen that the mullite crystals in AAFA under both curing methods showed similar morphologies, i.e., loosely stacked thin plates. However, relatively smaller crystals are identified under microwave curing (Fig. 10a-1) compared to those under thermal oven curing (Fig. 10a-2). The selected-area electron diffraction (SAED) patterns further confirm that the thin plates in both figures are crystalline. It should be noted that both mullite crystals and the amorphous phases in

fly ash are originated from the clay constitute of coal. During the combustion of coal, the clay constituents melt, and form suspended alumina-silica droplets. Upon rapid cooling in the exhaust gases, only part of the droplets crystallizes to form mullites, whilst the rest which does not crystallize forms the amorphous phases in fly ash and contributes to the reactivity of fly ash. As a result, the mullite is usually intermixed with amorphous phase in fly ash particles [48]. Therefore, the mullite crystals can be exposed only if the surrounding amorphous phases have been dissolved during the early stage of the reaction. From Fig. 10, it can be noticed that the mullite plates under both curing techniques can be clearly seen, indicating that reasonable dissolution of amorphous alumina-silica phases has been achieved regardless of the curing methods adopted. However, a further comparison of the mullite crystals obtained from the two curing methods as shown in Fig. 10b-1 and Fig. 10b-2 indicates that less amorphous phase can be noticed from the AAFA cured with microwave heating. Considering the much-reduced duration of microwave curing, this implies that microwaves can significantly increase the dissolution process of fly ash in AAFA. On the other hand, it can be deduced that the diffusion process must have also been enhanced. Otherwise, the mullite plates should still be embedded in the dissolved silica and alumina species.

3.3.3. MIP

The pore size distributions of the two AAFA samples are presented in Fig. 11. The total porosity of OV24 and MW30 are 28.5 % and 28.1 % respectively. Although their total porosities were very close, OV24 demonstrated a finer pore size distribution than MW30. Normally, the pore size distribution could be divided into three regions. The pores range of <100 nm are classified as small pores, whilst the pores ranges of 100–500 nm (medium) and > 500 nm (large) are attributed to capillary pores [51]. In the current study, there existed a small amount (4.0 %) of the fine pores in the pore size range of <100 nm in OV24; in comparison, there were little pores identified in this region in MW30. In the pore size range of 100–500 nm, the pores in OV24 (52.1 %) are more than twice than that in MW30 (24.1 %). However, in the pore size range of >500 nm, there was 75.9 % pores accounting for capillarity pores in MW30, compared to 43.5 % in OV24. Therefore, compared to thermal oven curing, the MIP results indicate that the AAFA cured with microwave appeared to have a more porous structure. This finding is consistent with the observations from SEM and TEM, which is also in agreement with
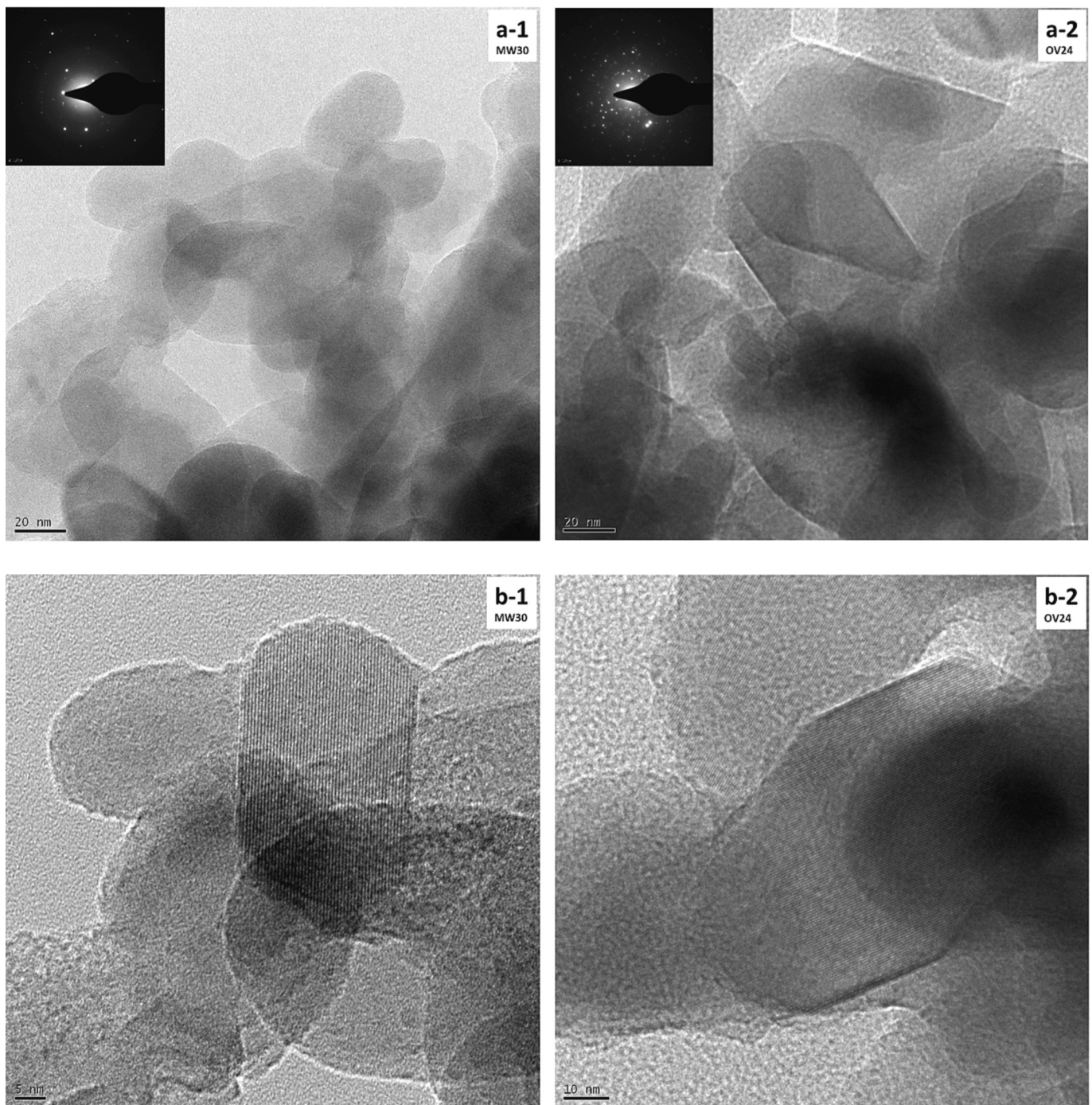
Fig. 10. TEM images and SAED patterns of mullite in AAFA: (a1-b1) MW30 and (a2-b2) OV24.

the finding reported in other research [52]. Additionally, the denser structure of OV24 could have also contributed to the higher compressive strength identified in this study.
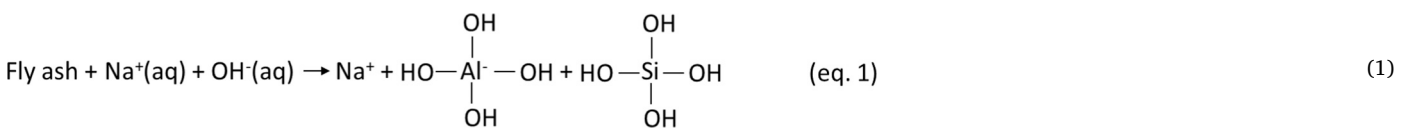
4. Discussion

In the past couple of decades, microwave heating has been increasingly recognised as a promising alternative low-carbon curing technique for cementitious materials. In particular, its potential application in manufacturing AAFA has attracted lots of attention since the production of AAFA, especially, NaOH-activated AAFA, often requires thermal curing which may offset the low-carbon nature of AAFA itself. It has been widely believed in the literature that the dominant contribution of

microwave heating to the reaction of AAFA can be attributed to its volumetric heating and, as a result, the AAFA can be cured within a short period of time with much less consumption of energy. However, based on the pulsed microwave regime adopted in this study the highest temperature reached in the AAFA sample (MW30) was measured to be 125 °C, whilst that in the AAFA cured with thermal oven (OV24) was 77.7 °C. Since the pulsed microwave curing only lasted for 1 h (however, the effective microwaving time actually lasted for only 3 min), even if we consider this highest temperature can be maintained throughout the whole 1-hour duration of the pulsed microwave curing, the maturity [53] (i.e. the product of temperature and time) is only 125 °C·h. As the thermal oven curing lasted for 24 h, if we again assume that the highest temperature could be maintained throughout the whole curing duration,

it will give a maturity of 1864.8 °C·h. This indicates that the maturity of MW30 is only 6.7 % of that of OV24. Obviously, the above calculation is just a rough estimation. However, due to the very short duration of the microwave curing, there is no doubt that a big difference in the maturity between these two curing methods is unavoidable. With such a big difference existing in maturity, it is not convincing to claim that it is just the thermal effect of microwaves that has resulted in the 82 % of the compressive strength and 74 % (based on TG results, however, this could even reach 96 % based on HCl method) of the reaction products of those of OV24 were developed by microwave curing within such a short period of time. Surely, something else must have contributed to such a rapid development in compressive strength and reaction products of microwave-cured AAFA. To understand the possible mechanisms involved within such a short period of time, a good understanding of the kinetics (such as calorimetric data) involved in each curing method would be essential.

In an attempt to understand the kinetics involved in AAFA cured by thermal oven, an ICC test was carried out as this is most accepted technique for investigating the kinetics of cementitious materials. Fig. 12 shows the ICC curve of the AAFA cured at 85 °C for 24 h. As can be seen, after the fly ash was in contact with 8 M NaOH solution, an intense liberation of heat was observed at 10–11 min (i.e., the first peak on the ICC curve). The rate of reaction then slowed down and the liberation of heat was reduced and maintained, showing the typical feature of '***induction***'. After a short induction period, the rate of reaction started to accelerate after 28–29 min and reached a maximum heat flow (i.e., the second peak on the ICC curve) at 41–42 min. Followed by this, the reaction rate slowed down gradually and then maintained at a very low level during the rest of the time until 24 h. It is interesting to notice that, in general, the above pattern is very similar to that obtained from the hydration of C_3S (even though there are significant differences in the chemistry involved between the reaction of AAFA and C_3S). It is worth highlighting that based on the well-established cement chemistry, the kinetics of C_3S is normally divided into five periods, namely, ***pre-induction***, ***induction***, ***acceleration***, ***deceleration*** and ***diffusion*** periods [54]. Drawing upon this well-established knowledge on C_3S hydration, the ICC result in Fig. 12 has, therefore, been divided into five periods, accordingly, due to the similarity in the ICC curves between the two systems. Based on the understanding which has been developed in the literature on the early reaction of AAFA [55], the possible reactions/ mechanisms associated with each period are given below.

In the ***pre-induction period***, the covalent Si—O—Si, Si—O—Al and Al—O—Al bonds in fly ash are broken in the highly alkaline environment, resulting in the dissolution of reactive silica and alumina species from the raw fly ash as shown by Eq. (1) [56] below.

passivating the surface of fly ash by preventing the access of hydroxyl ions to fly ash [59]. It is mainly due to this passivation process, the dissolution of fly ash is significantly reduced, leading to the ***induction period*** and slowdown of the reaction of AAFA as shown in Fig. 12. However, when a critical point (i.e., supersaturation) is reached, the growth of principle reaction products starts to accelerate [58,60] (i.e., ***acceleration period***) and the three-dimensional structure of the N-A-S-H gel is to be formed with tetrahedra of Si and tetrahedra of Al [5] during this period. With continued precipitation of N-A-S-H gel on the surface of fly ash particles [5], the rate of reaction decreases (i.e., ***deceleration period***). Followed by this, the microstructure around the unreacted fly ash particles is gradually densified and the initial strength is developed [5]. At this stage, the reaction is believed to be governed by diffusion (i. e., ***diffusion period***).

To understand the kinetics of AAFA reaction in microwave curing, it is desirable that an ICC result similar to Fig. 12 should be obtained for the AAFA under microwave curing. Unfortunately, to the best knowledge of the authors, this technology is currently unavailable. However, since the strength development is normally associated with the diffusion period (i.e., strength can only start to develop at diffusion period), the strength gained after different microwave curing cycles have been marked on the ICC curve in Fig. 12, together with those obtained at different curing durations from thermal oven curing at 85 °C. It can be seen that, under thermal oven curing, the AAFA developed 2.50 MPa compressive strength after 2 h thermal oven curing (i.e., in the diffusion period). This is then followed by 28.28 MPa at 4 h, 40.29 MPa at 7 h and 58.90 MPa at 24 h. These results are in good agreement with the well-establish knowledge of cement chemistry, i.e., the strength gain only occurs in the deceleration period [54]. In contrast, the strength of AAFA under microwave curing reached 28.16 MPa after only 20 min curing (10 cycles), which is then followed by 37.64 MPa at 40 min (20 cycles), 48.30 MPa at 60 min (30 cycles) and 46.63 MPa at 80 min (40 cycles). As the 28.16 MPa compressive strength was reached at 20 min, which is located within the pre-induction period of ICC curve obtained in thermal oven curing (as shown in Fig. 12), it can be deduced that the kinetics of the AAFA cured under microwave curing must have been significantly accelerated, i.e., all the five periods of AAFA under microwave curing must have been shifted significantly to the left as compared to the ICC curve obtained from thermal oven curing. Such a significant acceleration of the kinetics of reaction cannot be simply explained by the volumetric heating (i.e., thermal effect) of microwave alone. Based on the above analysis of the ICC results, together with the microstructure, reaction products and compressive strength results presented previously, it is the authors' opinion of this paper that, in addition to the thermal effect, the non-thermal effect of microwaves has also played an important role during the reaction process of AAFA. Since it is widely

$$\text{Fly ash} + \text{Na}^+(aq) + \text{OH}^-(aq) \longrightarrow \text{Na}^+ + \underset{\displaystyle \overset{\textstyle OH}{|}}{\overset{\displaystyle \overset{\textstyle OH}{|}}{HO-Al^--OH}} + \underset{\displaystyle \overset{\textstyle OH}{|}}{\overset{\displaystyle \overset{\textstyle OH}{|}}{HO-Si-OH}} \qquad \text{(eq. 1)} \tag{1}$$

It is generally considered that the dissolution of fly ash (as shown in Eq. (1)) and subsequent release of reactive silica and alumina from fly ash particles is the very first step of the alkaline activation of fly ash [17]. However, due to the lower bond energy of Al—O bond (501.9 ± 10.6 kJ/mol) as compared to that of the Si—O bond (799.6 ± 13.4 kJ/ mol) [57], the early dissolution of fly ash in AAFA is dominated by the preferential dissolution of Al from fly ash particles. Due to this preferential dissolution of Al, a siliceous layer is formed on the surface of fly ash particles [58]. Because of the formation of this siliceous layer, the dissolved Al species then adsorb to the surface of fly ash particles,

accepted that the hydration kinetics of cementitious materials is mainly controlled by ***dissolution***, ***diffusion***, ***nucleation*** and ***growth*** mechanisms [60], by drawing upon the recent findings from synthesising zeolites from fly ash using microwaves [4,61], the possible effects that microwave curing (both thermal and non-thermal effects) may have on the above four mechanisms, and hence the kinetics of the reaction of AAFA, are proposed and compared with those under the thermal oven curing, respectively. The details are further discussed and elaborated, separately, below.
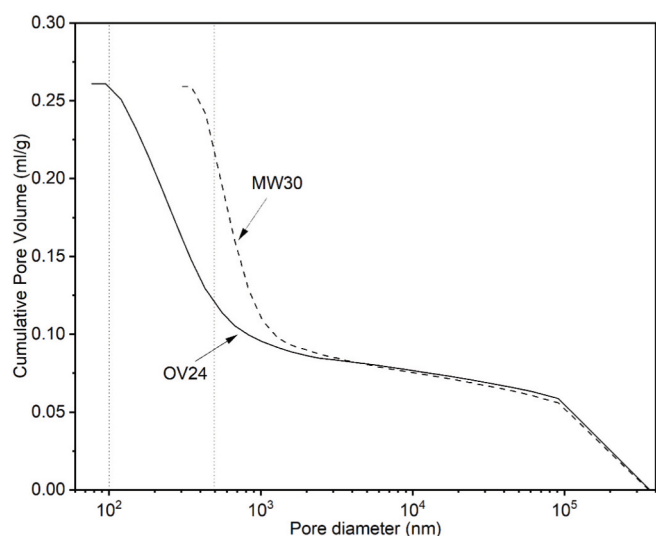
a. Cumulative porosity curves
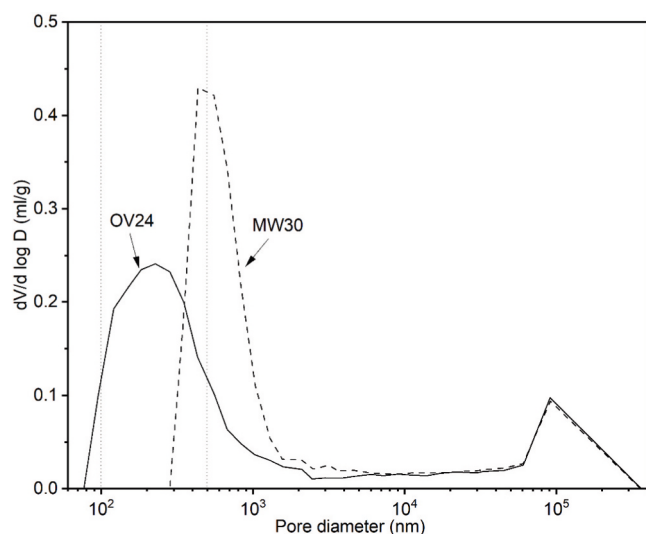
b. Derivative porosity curves

Fig. 11. Pore size distribution of AAFA.

1) Effect of microwave curing on the dissolution mechanism of AAFA

As indicated in Fig. 13, due to the different heating mechanisms between thermal oven and microwave curing, different temperature profiles can be developed within the fly ash particles at the early stage of reaction. As discussed before, the dominant heating mechanism of the thermal oven is thermal conduction. As a result, the surface of the fly ash particles is initially heated from the outside to the inside, whilst the temperature at the core of the fly ash particle is low. Over time, the temperature of the core is increased. Consequently, the dissolution of the reactive silica and alumina is slow at the early stage of reaction under thermal oven curing. On the contrary, microwaves can heat the fly ash particles volumetrically. Different from the thermal oven cured fly ash, the fly ash under microwave curing is heated from inside of the fly ash particles with the highest temperature being quickly reached inside the fly ash particle. This can accelerate the dissolution of the reaction silica and alumina from the inside of the fly ash particles, even with a possibility of causing the rupture of fly ash particles, which has been clearly demonstrated by the TEM image in Fig. 8a.

2) Effect of microwave curing on the diffusion mechanism of AAFA

Due to the preferential dissolution of Al, a siliceous layer is formed on the surface of fly ash particles. The dissolved Al species then adsorb to the surface of fly ash particles, passivating the surface of fly ash by preventing the access of hydroxyl ions to fly ash [59] (as shown in Fig. 14). Thus, the dissolution of fly ash is significantly reduced, leading to the induction period and slowdown of the reaction of AAFA. This explains why a long curing duration is needed for the conventional thermal curing (such as thermal oven curing). In contrast, under microwave curing, due to its non-thermal effects, not only the dissolution of the amorphous silica and alumina is increased [33,34] (as explained above), the diffusion of the dissolved Si and Al species is also accelerated [4,33,35]. This, in particular, can benefit the migration of the dissolved aqueous Al away from the vicinity of the fly ash particles at the early stage of reaction (as shown in Fig. 14), preventing/reducing the adsorption of Al species on the surface of fly ash particles. As a result, the passivation (and hence the induction period) induced by the adsorption of Al species is much reduced under microwave curing, leading to a continuous dissolution of fly ash particles – this can mechanistically explain the fast reaction observed from the microwave cured AAFA within a short curing duration. However, different from the above passivation theory, recent studies considered that the occurrence of the induction period and the slowdown of the hydration reaction can be mainly attributed to and determined by the degree of undersaturation of the dissolved species [62]. Based on this theory, during the initial hydration, the degree of the undersaturation of the dissolved species is high, consequently the rate of dissolution is high. However, with continued reaction, the concentration of the species dissolved in solution continues to increase and the reaction slows down. Therefore, in the current study, the slow diffusion process of the dissolved ions, in particular, the alumina species, at the early stage of reaction under thermal oven curing can result in a build-up of the alumina species in the vicinity of fly ash particles, which can result in a reduced degree of the undersaturation and, thus, a reduced dissolution of fly ash. On the contrary, under microwave curing, the diffusion of the dissolved silica and alumina species (in particular, alumina species) is increased and therefore a higher degree of undersaturation of the dissolved species can be maintained within the immediate vicinity of fly ash particles. This, in turn, can ensure that a higher degree of dissolution can be maintained. Regardless of the theories to be applied, it is believed that it is mainly because of the non-thermal effects of microwaves and, thus, the increased diffusion of the dissolved silica and alumina species (as schematically shown in Fig. 14 below) that have contributed to the continuous dissolution of fly ash particles and subsequent fast reaction of AAFA under microwave curing.

3) Effect of microwave curing on the nucleation mechanism of AAFA

It is widely accepted that, regardless of the curing methods, with the increased dissolution of the reactive silica and alumina over time, gelation and thus the nuclei start to be formed in AAFA [5,58]. However, under the thermal oven curing, due to the adsorption of the initially dissolved alumina on the surfaces of fly ash particles, the nuclei are mainly formed on the surface and the immediate vicinity of the fly ash particles [58]. In contrast, as schematically demonstrated in Fig. 15, under the microwave curing, due to the enhanced diffusion of the dissolved silica and alumina caused by the non-thermal effects of microwaves, the nuclei are mainly formed in the spaces between the fly ash particles (as directly supported by the SEM images shown in Fig. 7b-1 and d-1).

4) Effect of microwave curing on the growth mechanism of AAFA

Following the nucleation, the growth/precipitation of the N-A-S-H gel then follows [5,58]. As schematically shown in Fig. 16 below, in the
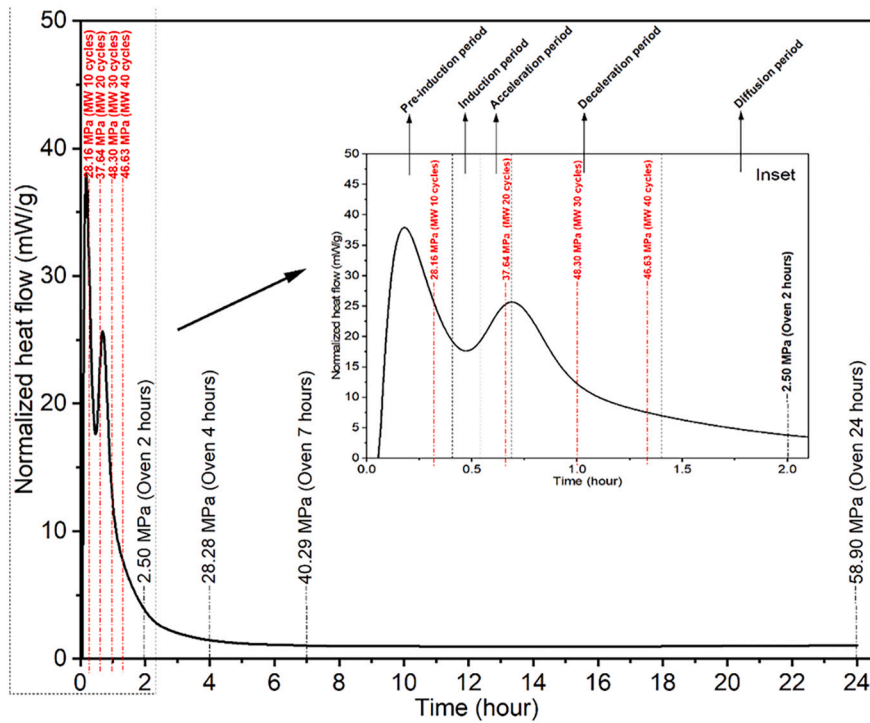
Fig. 12. ICC curve of AAFA at 85 °C.

case of thermal oven curing, due to the precipitation of the nuclei on/near the surface of fly ash particles, the growth of N-A-S-H gel and zeolite crystals are mainly initiated from the surface of the fly ash particles and then grow outwards [63,64]. In addition, as the surface of fly ash particles is covered by a thick Al-rich products, the initially formed products, Gel 1, is an Al-rich N-A-S-H gel which can only be transferred to Gel 2, a Si-rich N-A-S-H gel, at later stage of reaction. However, due to this thick layer of products formed on the surface of fly ash particles, further access of the hydroxyl ions and, hence, the reaction of fly ash could be hindered [58]. As a result, similar to the hydration products formed in PC [65], the inner reaction products with some denser and finer pores are formed near the surface of fly ash particles, whilst the outer products with more porous and coarser pores are formed away from the fly ash particles, filling the space between the fly ash particles. This hypothesis can be fully supported and verified by the observations from the TEM images in Fig. 9d-2. Therefore, the fine pores in the pore

size range of <100 nm formed in OV24 (as shown in Fig. 11) can be presumably attributed to the formation of inner products under thermal curing. However, under the microwave curing, due to the distributed formation of the nuclei between fly ash particles, the growth of the N-A-S-H gel is mainly focused in the region between fly ash particles, which can be verified by SEM images in Fig. 7b-1 and d-1. In addition, since the initially formed Al-rich nuclei are distributed, the Si/Al ratio (1.81 as shown in Fig. 9c-1) of the subsequently formed N-A-S-H under microwave curing is, consequently, higher than the typical Gel 1, but close to the typical Gel 2 as reported in the literature [56]. Due to the short curing duration under the microwave curing and the relatively higher Si/Al ratio, this gel could be temporarily stabilised as noticed in this study. On the other hand, the much-improved crystallisation of hydroxysodalite and chabazite-Na in MW30 could also support the hypothesis that the growth of N-A-S-H and zeolites are mainly occurred in the space between fly ash particles because zeolites request more space
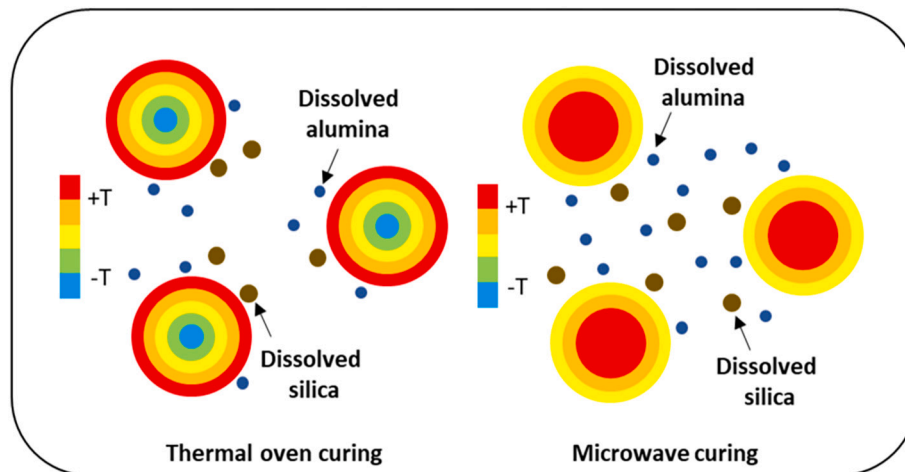

Fig. 13. Schematic diagram showing the dissolution process of fly ash in NaOH-activated AAFA under thermal oven curing and microwave curing.
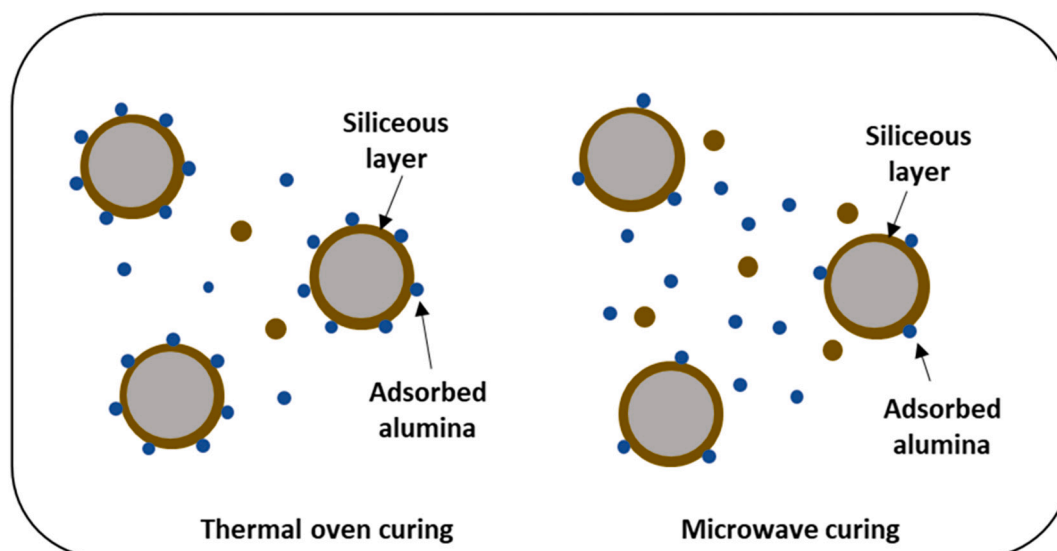
Fig. 14. Schematic diagram showing the diffusion process of the dissolved silica and alumina species in NaOH-activated AAFA under thermal oven curing and microwave curing.

to form a better crystalline structure, an environment which is impossible to be obtained in the immediate vicinity of fly ash under the thermal curing.

Whilst the above discussion and possible mechanisms as schematically shown in Figs. 13-16 can give a reasonable explanation to the results presented in this paper, however, the extremely fast strength development of AAFA cured under the microwave curing would imply that some additional mechanisms must have also facilitated or promoted the nucleation and growth processes of N-A-S-H gel in addition to the enhanced dissolution and diffusion caused by the non-thermal effects of microwaves since both nucleation and growth processes have been considered as rate-controlling factors [54,60]. Otherwise, it is impossible for MW30 to develop such a high strength within one hour. It has been reported that the activation energy of ^{18}O bulk diffusion in sapphire under microwave radiation was only 60 % of that under conventional heating [66]. Other researchers have also reported that microwave radiation could reduce the activation energy [67,68]. Drawing upon all these related findings, it is the authors' opinion that to accomplish the nucleation and growth of N-A-S-H gel needed within one hour in order to develop the microstructure and strength properties observed under the microwave curing in this study, the activation energy of AAFA under microwave curing might have also been reduced. Although this is a reasonable hypothesis based on the results presented in this paper, research is still needed to fully verify this in the future. On the other hand, even though the results reported in this paper shows a great potential of curing AAFA with microwave heating, a domestic microwave oven with pulsing ratio and power level manually controlled (as adopted in this paper) is not applicable for industry. Bespoke microwave oven with temperature monitoring system needs to be developed for further research.

5. Conclusions

The reaction products and the microstructure of a microwave-cured *NaOH-activated AAFA* were investigated in this paper in order to develop some theoretical understanding to explain why a high early strength can be developed by microwave curing within a very short period of curing duration. Based on the results and discussion presented in this paper, the following conclusions can be drawn:

- The formation of an Al-rich N-A-S-H gel and crystalline chabazite-Na were favoured under the microwave curing, whilst a Si-rich N-A-S-H gel and crystalline hydroxysodalite were dominant under the thermal oven curing.

- The N-A-S-H gels formed under the microwave curing and the thermal oven curing presented a crumpled foil-like morphology. However, the Al-rich N-A-S-H gel formed under the microwave curing showed a coarser and porous structure, compared to the finer and compacted Si-rich N-A-S-H gel formed under the thermal oven curing. Furthermore, the flaky Al-rich N-A-S-H gel from the microwave cured AAFA sample showed an interwoven structure with a relatively, uniformly distributed texture, whilst the fibrillar Si-rich N-A-S-H gel from the thermal oven cured AAFA demonstrated a denser inner product and a loose outer product.

- The reaction products formed under the microwave curing mainly precipitated in the regions between fly ash particles, whereas those under the thermal oven curing are mainly formed on the surface/in the close vicinity of fly ash particles.

- Although the total porosities of the AAFAs cured under the microwave curing and the thermal oven curing were very close, the microwave cured AAFA appeared to have a more porous structure than the thermal oven cured AAFA.

- The fast strength development under the microwave curing can be attributed not only to the thermal effect of microwaves which can increase the temperature of AAFA due to the volumetric heating generated by microwaves, but also to the non-thermal effects of microwaves which can promote the dissolution and diffusion of silica and alumina species during the AAFA reaction process. Furthermore, the non-thermal effects of microwaves may have also facilitated or promoted the nucleation and growth processes of N-A-S-H gel and crystalline phases.

CRediT authorship contribution statement

Shi Shi: Conceptualization, Methodology, Formal analysis, Investigation, Data curation, Writing – original draft. **Hui Li:** Conceptualization, Resources, Writing – review & editing, Supervision, Funding acquisition. **Qizhi Zhou:** Methodology, Investigation, Writing – review & editing. **Hongzhou Zhang:** Formal analysis, Investigation, Data curation. **P.A.M. Basheer:** Resources, Writing – review & editing, Supervision. **Yun Bai:** Conceptualization, Methodology, Resources, Writing – review & editing, Supervision, Funding acquisition.
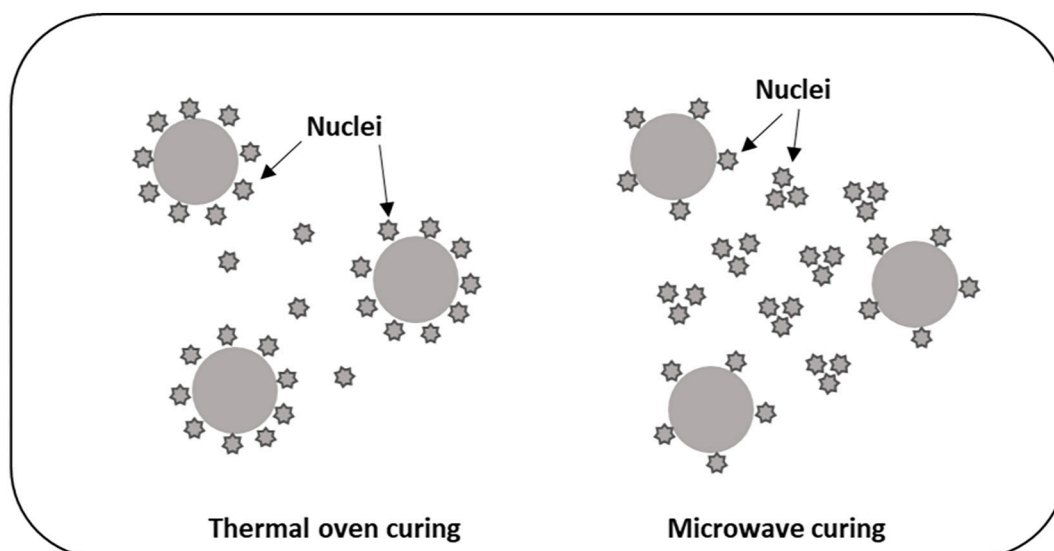
Fig. 15. Schematic diagram showing the nucleation process of NaOH-activated AAFA under thermal oven curing and microwave curing.
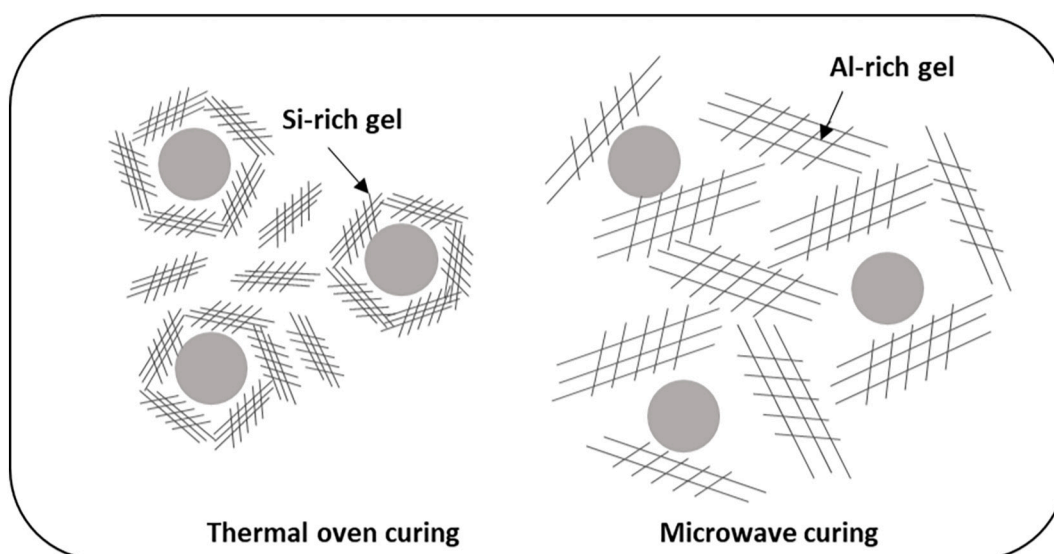

Fig. 16. Schematic diagram showing the growth process of NaOH-activated AAFA under thermal oven curing and microwave curing.

Declaration of competing interest

The authors declare that they have no known competing financial interests or personal relationships that could have appeared to influence the work reported in this paper.

Data availability

Data will be made available on request.

Acknowledgements

References

[1] A.R.K. Gollakota, V. Volli, C.M. Shu, Progressive utilisation prospects of coal fly ash: a review, Sci. Total Environ. 672 (2019) 951–989.
[2] A. Palomo, M.W. Grutzeck, M.T. Blanco, Alkali-activated fly ashes - a cement for the future, Cem. Concr. Res. 29 (8) (1999) 1323–1329.
[3] J.L. Provis, A. Palomo, C.J. Shi, Advances in understanding alkali-activated materials, Cem. Concr. Res. 78 (2015) 110–125.
[4] J.K. Kim, H.D. Lee, Effects of step change of heating source on synthesis of zeolite 4A from coal fly ash, J. Ind. Eng. Chem. 15 (5) (2009) 736–742.
[5] A. Fernandez-Jimenez, A. Palomo, M. Criado, Microstructure development of alkali-activated fly ash cement: a descriptive model, Cem. Concr. Res. 35 (6) (2005) 1204–1209.
[6] E. Álvarez-Ayuso, et al., Environmental, physical and structural characterisation of geopolymer matrixes synthesised from coal (co-)combustion fly ashes, J. Hazard. Mater. 154 (1–3) (2008) 175–183.
[7] T. Bakharev, Geopolymeric materials prepared using class F fly ash and elevated temperature curing, Cem. Concr. Res. 35 (6) (2005) 1224–1232.
[8] Z. Zuhua, et al., Role of water in the synthesis of calcined kaolin-based geopolymer, Appl. Clay Sci. 43 (2) (2009) 218–223.
[9] M. Criado, et al., Effect of the SiO2/Na2O ratio on the alkali activation of fly ash. Part II: 29Si MAS-NMR survey, Microporous Mesoporous Mater. 109 (1–3) (2008) 525–534.

[10] A. Fernandez-Jimenez, et al., The role played by the reactive alumina content in the alkaline activation of fly ashes, Microporous Mesoporous Mater. 91 (1–3) (2006) 111–119.

[11] A. Katz, Microscopic study of alkali-activated fly ash, Cem. Concr. Res. 28 (2) (1998) 197–208.

[12] F. Puertas, et al., Mechanical and durable behaviour of alkaline cement mortars reinforced with polypropylene fibres, Cem. Concr. Res. 33 (12) (2003) 2031–2036.

[13] A. Criado, A. Palomo, A. Fernandez-Jimenez, Alkali activation of fly ashes. Part 1: effect of curing conditions on the carbonation of the reaction products, Fuel 84 (16) (2005) 2048–2054.

[14] G.C. Long, A. Omran, Z.M. He, Heat damage of steam curing on the surface layer of concrete, Mag. Concr. Res. 64 (11) (2012) 995–1004.

[15] A.C. Metaxas, R.J. Meredith, in: R.J. Meredith (Ed.), Industrial Microwave Heating, Peregrinus on behalf of the Institution of Electrical Engineers, London, 1983.

[16] N. Makul, et al., Microwave-assisted heating of cementitious materials: relative dielectric properties, mechanical property, and experimental and numerical heat transfer characteristics, Int. Commun. Heat Mass Transfer 37 (8) (2010) 1096–1105.

[17] K.C.G. Ong, A. Akbarnezhad, Microwave-Assisted Concrete Technology: Microwave-Assisted Concrete Technology, CRC Press, Boca Raton, 2015.

[18] A. Watson, Curing of concrete, in: E.C. Okress (Ed.), Microwave Power Engineering, volume 2, Academic Press, New York, 1968, pp. 108–110.

[19] X.Q. Wu, J.G. Dong, M.S. Tang, Microwave curing technique in concrete manufacture, Cem. Concr. Res. 17 (2) (1987) 205–210.

[20] R.G. Hutchison, et al., Thermal acceleration of Portland cement mortars with microwave energy, Cem. Concr. Res. 21 (5) (1991) 795–799.

[21] C.K.Y. Leung, T. Pheeraphan, Microwave curing of Portland-cement concrete - experimental results and feasibility for practical applications, Constr. Build. Mater. 9 (2) (1995) 67–73.

[22] C.K.Y. Leung, T. Pheeraphan, Determination of optimal process for microwave curing of concrete, Cem. Concr. Res. 27 (3) (1997) 463–472.

[23] P. Rattanadecho, et al., Development of compressive strength of cement paste under accelerated curing by using a continuous microwave thermal processor, Mater. Sci. Eng. A 472 (1–2) (2008) 299–307.

[24] N. Makul, P. Rattanadecho, A. Pichaicherd, Accelerated microwave curing of concrete: a design and performance-related experiments, Cem. Concr. Compos. 83 (2017) 415–426.

[25] Y.N. Kong, et al., Hydration and microstructure of cement-based materials under microwave curing, Constr. Build. Mater. 114 (2016) 831–838.

[26] A. Graytee, J.G. Sanjayan, A. Nazari, Development of a high strength fly ash-based geopolymer in short time by using microwave curing, Ceram. Int. 44 (7) (2018) 8216–8222.

[27] P. Chindaprasirt, U. Rattanasak, S. Taebuanhuad, Role of microwave radiation in curing the fly ash geopolymer, Adv. Powder Technol. 24 (3) (2013) 703–707.

[28] J. Somaratna, D. Ravikumar, N. Neithalath, Response of alkali activated fly ash mortars to microwave curing, Cem. Concr. Res. 40 (12) (2010) 1688–1696.

[29] K. Konig, et al., Evaluation of locally available amorphous waste materials as a source for alternative alkali activators, Ceram. Int. 47 (4) (2021).

[30] Y.F. Ling, K.J. Wang, C.Q. Fu, Shrinkage behavior of fly ash based geopolymer pastes with and without shrinkage reducing admixture, Cem. Concr. Compos. 98 (2019) 74–82.

[31] G.S. Wang, Y.W. Ma, Drying shrinkage of alkali-activated fly ash/slag blended system, J. Sustain. Cem. Based Mater. 7 (4) (2018) 203–213.

[32] M. Criado, A. Fernandez-Jimenez, A. Palomo, Alkali activation of fly ash: effect of the SiO2/Na2O ratio part I: FTIR study, Microporous Mesoporous Mater. 106 (1–3) (2007) 180–191.

[33] S.S. Bukhari, et al., Conversion of coal fly ash to zeolite utilizing microwave and ultrasound energies: a review, Fuel 140 (2015) 250–266.

[34] R. Anuwattana, et al., Conventional and microwave hydrothermal synthesis of zeolite ZSM-5 from the cupola slag, Microporous Mesoporous Mater. 111 (1–3) (2008) 260–266.

[35] B.I. Whittington, N.B. Milestone, The microwave-heating of zeolites, Zeolites 12 (7) (1992) 815–818.

[36] S. Gunasekaran, H.W. Yang, Effect of experimental parameters on temperature distribution during continuous and pulsed microwave heating, J. Food Eng. 78 (4) (2007) 1452–1456.

[37] S. Gunasekaran, H.W. Yang, Optimization of pulsed microwave heating, J. Food Eng. 78 (4) (2007) 1457–1462.

[38] C.J. Shi, A.F. Jimenez, A. Palomo, New cements for the 21st century: the pursuit of an alternative to Portland cement, Cem. Concr. Res. 41 (7) (2011) 750–763.

[39] P. Arjuan, M.R. Silbee, D.M. Roy, Quantitative determination of the crystalline and amorphous phases in low calcium fly ashes, in: Proceeding of the 10th International Congress of the Chemistry of Cement, 1997. Gothenburg, Sweden.

[40] A. Fernandez-Jimenez, Quantitative determination of phases in the alkali activation of fly ash. Part I. Potential ash reactivity, Fuel 85 (5-6) (2006) 625–634.

[41] A. Fernandez-Jimenez, Quantitative determination of phases in the alkaline activation of fly ash. Part II: Degree of reaction, Fuel 85 (14-15) (2006) 1960–1969.

[42] M. Criado, et al., An XRD study of the effect of the SiO2/Na2O ratio on the alkali activation of fly ash, Cem. Concr. Res. 37 (5) (2007) 671–679.

[43] A. Fernandez-Jimenez, A. Palomo, Mid-infrared spectroscopic studies of alkali-activated fly ash structure, Microporous Mesoporous Mater. 86 (1–3) (2005) 207–214.

[44] F. Winnefeld, et al., Assessment of phase formation in alkali activated low and high calcium fly ashes in building materials, Constr. Build. Mater. 24 (6) (2010) 1086–1093.

[45] I.E. Yuzay, et al., Effects of synthetic and natural zeolites on morphology and thermal degradation of poly(lactic acid) composites, Polym. Degrad. Stab. 95 (9) (2010) 1769–1777.

[46] D.D.B. Nergis, et al., XRD and TG-DTA study of new alkali activated materials based on Fly ash with sand and glass powder, Materials 13 (2) (2020).

[47] A. Fernandez-Jimenez, A. Palomo, Composition and microstructure of alkali activated fly ash binder: effect of the activator, Cem. Concr. Res. 35 (10) (2005) 1984–1992.

[48] H. Li, et al., Microstructure and performance of fly ash micro-beads in cementitious material system, Constr. Build. Mater. 52 (2014) 422–427.

[49] Z.W. Peng, et al., Microwave power absorption in materials for ferrous metallurgy, JOM 69 (2) (2017) 178–183.

[50] A.V. Girao, et al., Composition, morphology and nanostructure of C-S-H in 70% white Portland cement-30% fly ash blends hydrated at 55 degrees C, Cem. Concr. Res. 40 (9) (2010) 1350–1359.

[51] Y. Ma, J. Hu, G. Ye, The pore structure and permeability of alkali activated fly ash, Fuel 104 (2013) 771–780.

[52] H. Shi, et al., Effect of microwave curing on metakaolin-quartz-based geopolymer bricks, Constr. Build. Mater. 258 (2020).

[53] A.M. Neville, Properties of Concrete, 5th ed., Prentice Hall, Harlow, 2011.

[54] J. Bensted, P. Barnes, Structure and Performance of Cements, 2nd ed., Taylor & Francis e-Library, 2008.

[55] S. Shi, Multi-stage Microwave Curing for Manufacturing Alkali-activated Fly Ash, University College London, 2017.

[56] P. Duxson, et al., Geopolymer technology: the current state of the art, J. Mater. Sci. 42 (9) (2007) 2917–2933.

[57] A.G. Whittaker, A.R. Mount, M.R. Heal, Physical Chemistry, BIOS Scentific Publisher Limited, USA, 2000.

[58] C.A. Rees, et al., The mechanism of geopolymer gel formation investigated through seeded nucleation, Colloids Surf. A Physicochem. Eng. Asp. 318 (1–3) (2008) 97–105.

[59] R.K. Iler, Effect of adsorbed alumina on the solubility of amorphous silica in water, J. Colloid Interface Sci. 43 (2) (1973) 399–408.

[60] J.W. Bullard, et al., Mechanisms of cement hydration, Cem. Concr. Res. 41 (12) (2011) 1208–1223.

[61] Q. Tian, K. Sasaki, Application of fly ash-based geopolymer for removal of cesium, strontium and arsenate from aqueous solutions: kinetic, equilibrium and mechanism analysis, Water Sci. Technol. 79 (11) (2019) 2116–2125.

[62] P. Juilland, et al., Dissolution theory applied to the induction period in alite hydration, Cem. Concr. Res. 40 (6) (2010) 831–844.

[63] R.R. Lloyd, J.L. Provis, J.S.J. van Deventer, Microscopy and microanalysis of inorganic polymer cements. 1: remnant fly ash particles, J. Mater. Sci. 44 (2) (2009) 608–619.

[64] R.R. Lloyd, J.L. Provis, J.S.J. van Deventer, Microscopy and microanalysis of inorganic polymer cements. 2: the gel binder, J. Mater. Sci. 44 (2) (2009) 620–631.

[65] I.G. Richardson, The nature of C-S-H in hardened cements, Cem. Concr. Res. 29 (8) (1999) 1131–1147.

[66] M.A. Janney, et al., Enhanced diffusion in sapphire during microwave heating, J. Mater. Sci. 32 (5) (1997) 1347–1355.

[67] A. de la Hoz, A. Diaz-Ortiz, A. Moreno, Microwaves in organic synthesis. Thermal and non-thermal microwave effects, Chem. Soc. Rev. 34 (2) (2005) 164–178.

[68] S. Nomanbhay, M.Y. Ong, A review of microwave-assisted reactions for biodiesel production, Bioengineering 4 (2) (2017) 57–78.